

High-throughput single-cell analysis reveals Omp38-specific monoclonal antibodies that protect against *Acinetobacter baumannii* infection

Yiwei Zhang, Hao Cheng, Peng Yu, Shufeng Wang, Hui Dong, Song Lu, Ruiqi Yang, Baiqing Li, Jie Luo, Ruihan Mao, Zhaohui Zhang, Yong Qi, Xiaohua Chen, Jinya Ding, Zemin He, Jingbo Zhang, Tingting Zhao, Xiangmei Chen, Rong Lin, Haibo Li, Yi Tian & Yuzhang Wu

To cite this article: Yiwei Zhang, Hao Cheng, Peng Yu, Shufeng Wang, Hui Dong, Song Lu, Ruiqi Yang, Baiqing Li, Jie Luo, Ruihan Mao, Zhaohui Zhang, Yong Qi, Xiaohua Chen, Jinya Ding, Zemin He, Jingbo Zhang, Tingting Zhao, Xiangmei Chen, Rong Lin, Haibo Li, Yi Tian & Yuzhang Wu (2025) High-throughput single-cell analysis reveals Omp38-specific monoclonal antibodies that protect against *Acinetobacter baumannii* infection, *Emerging Microbes & Infections*, 14:1, 2437243, DOI: [10.1080/22221751.2024.2437243](https://doi.org/10.1080/22221751.2024.2437243)

To link to this article: <https://doi.org/10.1080/22221751.2024.2437243>



© 2024 The Author(s). Published by Informa UK Limited, trading as Taylor & Francis Group



[View supplementary material](#)



Published online: 17 Dec 2024.



[Submit your article to this journal](#)



Article views: 645



[View related articles](#)



[View Crossmark data](#)

High-throughput single-cell analysis reveals Omp38-specific monoclonal antibodies that protect against *Acinetobacter baumannii* infection

Yiwei Zhang^{a*}, Hao Cheng^{b*}, Peng Yu^c, Shufeng Wang^a, Hui Dong^a, Song Lu^c, Ruiqi Yang^c, Baiqing Li^a, Jie Luo^d, Ruihan Mao^a, Zhaohui Zhang^a, Yong Qi^e, Xiaohua Chen^e, Jinya Ding^e, Zemin He^e, Jingbo Zhang^f, Tingting Zhao^c, Xiangmei Chen^g, Rong Lin^h, Haibo Li^b, Yi Tian^a and Yuzhang Wu^{a,c}

^aInstitute of Immunology, Third Military Medical University (Army Medical University), Chongqing, People's Republic of China;

^bDepartment of Microbiology and Biochemical Pharmacy, National Engineering Research Center of Immunological Products, College of Pharmacy, Third Military Medical University (Army Medical University), Chongqing, People's Republic of China; ^cChongqing International Institute for Immunology, Chongqing, People's Republic of China; ^dThe First Affiliated Hospital, Third Military Medical University (Army Medical University), Chongqing, People's Republic of China; ^eThe Second Affiliated Hospital, Third Military Medical University (Army Medical University), Chongqing, People's Republic of China; ^fGeneral Hospital of Central Theater Command, Wuhan, Hubei, People's Republic of China; ^gDepartment of Nephrology, Chinese PLA General Hospital, Chinese PLA Institute of Nephrology, National Key Laboratory of Kidney Diseases, National Clinical Research Center for Kidney Diseases, Beijing, People's Republic of China; ^hSanya People's Hospital, Sanya, People's Republic of China

ABSTRACT

Infections caused by *Acinetobacter baumannii* (*A. baumannii*) have emerged as a global public health concern because of high pathogenicity of this bacterium. Monoclonal antibodies (mAbs) have a lower likelihood of promoting drug resistance and offer targeted treatment, thereby reducing potential adverse effects; however, the therapeutic potential of mAbs targeting *A. baumannii* has not been fully characterized. In this study, mAbs against the outer membrane proteins (OMPs) of *A. baumannii* were isolated in a high-throughput manner. The ability of Omp38-specific mAbs to bind to *A. baumannii* strains from diverse sources was confirmed via enzyme-linked immunosorbent assay (ELISA). Intravenous administration of the Omp38-specific mAbs significantly improved the survival rate and reduced the bacterial load in a mouse model of lethal *A. baumannii* infection. Flow cytometry and ELISA confirmed that immune cell infiltration and cytokine production, respectively, decreased in a mouse model of sublethal *A. baumannii* infection. In addition, analysis of the Omp38-mAb C3 binding conformation revealed the potential mechanism of broad-spectrum binding activity of this mAb against *A. baumannii*. Taken together, these findings indicate that mAbs against Omp38 facilitate bacterial clearance from host, minimize inflammatory mediator release and reduce host damage, highlighting the potential of Omp38-specific mAbs in the clinical treatment of *A. baumannii* infection.

ARTICLE HISTORY Received 17 September 2024; Revised 22 November 2024; Accepted 28 November 2024

KEYWORDS *Acinetobacter baumannii*; outer membrane protein; monoclonal antibody; Beacon

Introduction

Acinetobacter baumannii (*A. baumannii*) is an opportunistic pathogen commonly found in the environment that is capable of causing severe infections in human tissues, such as the lungs and bloodstream, particularly in immunocompromised patients in the intensive care unit (ICU) [1,2]. Unlike typical gram-negative bacteria, *A. baumannii* possesses robust adhesion capabilities, facilitating its colonization at infection sites and enabling biofilm formation or cellular invasion [1]. Studies have reported a mortality rate of 56.2% among infected patients [2], prompting the World Health Organization (WHO) to classify *A. baumannii* as a priority 1 critical pathogen and

necessitating the urgent exploration of novel therapeutic strategies [1].

Antibiotics are considered the major treatment modality for *A. baumannii* infections [3]. However, *A. baumannii* is resistant to a wide range of antibiotics, including carbapenems and polymyxins, making treatment extremely difficult [4]. *A. baumannii* vaccines are safe, have few adverse effects and do not easily induce drug resistance [5]. However, owing to several factors, such as antigen sequence variability, no vaccine has succeeded in phase I clinical trials [6,7]. In recent years, monoclonal antibody (mAb) therapy has emerged as a promising approach for treating *A. baumannii* infections [8–11]. mAbs possess

CONTACT Haibo Li  lihaibo@tmmu.edu.cn; Yi Tian  tianyi@tmmu.edu.cn; Yuzhang Wu  wuyuzhang@tmmu.edu.cn, wuyuzhang@iicq.vip

*These authors contributed equally to this work.

 Supplemental data for this article can be accessed online at <https://doi.org/10.1080/22221751.2024.2437243>.

© 2024 The Author(s). Published by Informa UK Limited, trading as Taylor & Francis Group

This is an Open Access article distributed under the terms of the Creative Commons Attribution-NonCommercial License (<http://creativecommons.org/licenses/by-nc/4.0/>), which permits unrestricted non-commercial use, distribution, and reproduction in any medium, provided the original work is properly cited. The terms on which this article has been published allow the posting of the Accepted Manuscript in a repository by the author(s) or with their consent.

various advantages, such as increased safety and improved homology [12]. In addition, mAbs are less likely to promote drug resistance and offer targeted treatment, thereby reducing potential adverse effects [12]. Moreover, combining mAbs with antibiotics is a potential strategy to reduce antibiotic usage and mitigate the associated adverse effects [1].

Recent mAb development technologies have faced various challenges [13]. Hybridoma technology, for example, has issues such as reduced diversity due to competition between different hybridomas in the same culture [13,14]. Some non- or low-producing clones may exhibit a faster growth rate and outcompete the highly secreting clones [13,14]. Display selection technologies, including phage display, bacterial display, and yeast display, generate low-affinity mAbs because of the random pairings of the variable heavy (VH) and variable light (VL) regions [15–17]. These limitations render traditional approaches inefficient for antibody development. Recently, novel methods using microfluidic technology for direct B-cell antibody discovery have emerged [13,18–20]. The Beacon platform from Berkeley Lights enables single-cell manipulation, culture, and phenotypic analysis on nanofluidic chips and selectively exports the target cells on the basis of specific experimental outcomes [21–24]. This approach better preserves B-cell diversity, captures high-quality cells early in the discovery process and prevents the loss of promising clones. Following high-throughput screening, the selected cells can be extracted from the microfluidic chips to obtain natural VH and VL pairing sequences encoding the original antibodies [21–24].

A. baumannii contains a range of potential drug targets, including porin proteins, efflux pumps, outer membrane vesicles (OMVs), outer membrane proteins (OMPs), metal acquisition systems, secretion systems, phospholipases, and capsular polysaccharides [1,25,26]. The development of OMP-targeting mAbs has attracted increasing attention in recent years because of the distinctive roles of these proteins in facilitating bacterial adaptation to antibiotic- and host-induced stresses [9]. Vikas Kumar Goel et al. employed hybridoma technology to produce mAbs against *A. baumannii* iron-regulated outer membrane proteins (IROMPs), and the mAbs showed bactericidal and opsonizing activities against *A. baumannii* *in vitro* [9]. Omp38 (also known as OmpA), a prominent *A. baumannii* OMP, regulates *A. baumannii* adhesion, invasion, and biofilm formation [1,11,27] and contributes to inflammatory and other host responses [1,28]. In addition, Omp38 is not homologous to any proteins encoded by the human genome, which ensures that the administration of antibodies that inhibit Omp38 will not unnecessarily harm the host [29]. Furthermore, Omp38 overproduction has been reported to be a risk factor for nosocomial

pneumonia, bacteremia, and increased mortality rates in patients [30]. Given these factors, developing anti-Omp38 mAbs for use against *A. baumannii* infections is highly important.

In this study, mAbs targeting the OMPs of *A. baumannii* were obtained using high-throughput mAb isolation with the Beacon platform. We identified Omp38-specific mAbs, confirmed their binding to *A. baumannii* strains from diverse sources and demonstrated their encouraging therapeutic efficacy in lethal and sublethal infection models. In addition, the Omp38-mAb C3 binding conformation was predicted, suggesting the potential broad-spectrum capacity of mAb C3 to bind to *A. baumannii*.

Materials and methods

Ethics statement

All of the animal experiments were approved by the Animal Ethical and Experimental Committee of Army Medical University (Chongqing, China). Well-trained and skilled animal care personnel participated in the current study to minimize animal suffering.

Cells, animals and bacterial strains

The cells were cultured under a controlled atmosphere (37°C and 5% CO₂). 293 T cells were cultured in high-glucose Dulbecco's modified Eagle's medium (DMEM) (Gibco, 11965092) supplemented with 10% fetal bovine serum (FBS) (Gibco, A5256701), 100 U/mL penicillin, and 100 mg/mL streptomycin (Gibco, 15070063). RAW264.7 cells were cultured in high-glucose DMEM supplemented with 10% FBS, 100 U/mL penicillin, 100 µg/mL streptomycin, 2 mM L-glutamine (Gibco, A2916801), and 0.1 mg/mL Normocin (InvivoGen, ant-nr-05). A549 cells were cultured in Ham's F-12 K (Kaighn's) medium (Gibco, 21127022) supplemented with 10% FBS, 100 U/mL penicillin, and 100 mg/mL streptomycin. ExpiCHO cells were cultured in MetaCell CHO-310 medium (Cellplus Bio, L1013). Specific pathogen-free (SPF) female BALB/c mice and C57BL/6 mice aged 6–8 weeks were purchased from the Experimental Animal Center of Army Medical University. All the mice were kept under pathogen-free conditions in the animal center of Army Medical University. *A. baumannii* strains ATCC 17978 and LAC-4 were kindly provided by Prof. Yun Shi (West China Hospital, Sichuan University).

Preparation of the OMPs

A. baumannii ATCC 17978 was spread on Mueller Hinton agar solid culture media (24 g of Mueller Hinton agar solid powder, 15 g of agar powder and 1000

mL of ultrapure water) via the trilinear method and incubated in an incubator at 37°C for 12 hours. Single colonies were transferred to 20 mL of Mueller Hinton agar liquid culture media (24 g of Mueller Hinton agar and 1000 mL of ultrapure water) and cultured overnight at 37°C and 220 rpm for activation. The activated bacterial culture was then expanded to 1 L and cultured for 3 hours at 37°C and 220 rpm until the OD₆₀₀ reached 0.8. *A. baumannii* was subsequently resuspended in 10 mL of phosphate-buffered saline (PBS) (pH 7.2), and the bacteria were disrupted in a homogenizer for 10 minutes at a pressure of 750 bar. After centrifugation to remove the bacterial debris and sediment, the mixture was centrifuged again to collect the supernatant, which contained bacterial membrane proteins, including inner membrane proteins and OMPs. The membrane proteins were resuspended in 5 mL of 2% lauroyl sarcosine and incubated at 37°C for 30 minutes to dissolve the bacterial inner membrane proteins. The mixture was then centrifuged at 16,000 rpm for 1 hour to obtain the insoluble component, which contained the OMPs. The OMPs were purified according to a previous study [31]. After washing with 2 mL of 62.5 mM Tris HCl (pH 6.8), the OMPs were resuspended in 2 mL of 5% SDS and incubated at 4°C for 10 minutes. Methanol (6 mL) was added, and the mixture was vigorously vortexed and subsequently centrifuged at 12000rpm for 10 s. Then, 2 mL of chloroform was added, and the mixture was vigorously vortexed and centrifuged again at 12000rpm for 10 s. After the liquid phases had separated, 6 mL of ultrapure water was added, the mixture was vortexed vigorously and centrifuged at 12000rpm for 1 min, and the upper phase was discarded. Methanol (6 mL) was added to the lower phase, the mixture was vigorously vortexed and centrifuged at 9000 rpm for 2 minutes, the upper phase was discarded, and the resulting precipitate was the OMPs.

Expression of recombinant Omp38

A recombinant Omp38 plasmid for the Omp38 protein with 1 additional methionine in the 5' flank and 6 histidine tags in the 3' flank was constructed, cloned and inserted into pET30a for subsequent transformation into *E. coli* BL21 (DE3). The overexpressed Omp38 formed insoluble inclusion bodies, and the Omp38 was purified from the inclusion bodies via Ni-NTA affinity chromatography under denaturing conditions. Nickel column-bound Omp38 was eluted with imidazole gradient elution and detected by SDS-PAGE, which revealed the expected ~40 kDa band.

Mouse immunization

OMPs (50 µg) and 50 µL of QuickAntibody Mouse3W (Biodragon, KX0210042) were injected into the calf

muscles of 6–8 week-old BALB/c mice on days 0, 14, and 21. On the 21st day, a small amount of blood was collected from the tail vein for enzyme-linked immunosorbent assay (ELISA) determination of the serum OMP antibody titer. The mouse with the highest titer of anti-OMP antibodies was selected for further experiments. A final booster in normal saline was given intraperitoneally three days before the test with the Beacon system.

Isolation of single OMP-specific antibody-secreting cells (ASCs) via the Berkeley Lights Beacon system

Before the on-chip assay, biotinylated OMPs were coupled to streptavidin-coated assay beads (Berkeley Lights, 520-00053) at 4°C overnight to prepare conjugated beads. These beads were mixed with the fluorescently labeled anti-mouse secondary antibody (Alexa Fluor™ 568, Thermo Fisher, A-11004) at a 1:100 dilution in a total volume of 20 µL.

The ASCs were loaded onto OptoSelect 11k chips and cultured at 25°C in a novel plasmablast survival medium (Berkeley Lights, 75002051) designed to increase antibody secretion while maintaining cell viability [16,32]. Single-cell encapsulation was achieved by using OptoElectroPositioning (OEP) technology and optically transferring ASCs to nanoliter-sized chambers known as NanoPens. Thousands of ASCs were distributed into NanoPens across multiple chips via this light-based manipulation technique. An on-chip fluorescence-based assay was conducted to screen for antibodies that bind to the OMPs with measurements taken every 5 minutes for a total of 20 minutes at 36°C. Cells secreting antigen-specific antibodies were identified in the NanoPens adjacent to the fluorescent beads. After antigen-specific B cells were transferred from the NanoPens via OEP, the chips were washed with culture medium (2 minutes per cell). Then the cells were exported into individual wells of 96-well RT-PCR plates containing lysis buffer (Qiagen, 1070498) at 25°C.

Single B-cell sequencing and plasmid construction

After being exported from the Beacon system, the VH and VL sequences of the antibodies secreted by the OMP-binding B cells were amplified using the components of the Opto Plasma B Discovery cDNA Synthesis Kit (Berkeley Lights, 750-02030) [16]. RNA was isolated and purified from a single B-cell using Agencourt RNAClean XP beads (Beckman Coulter, A63987). Then, first-strand cDNA synthesis and total cDNA amplification were performed following the manufacturer's protocol (Berkeley Lights, 750-02030). The resulting total cDNA was purified using

Agencourt AMPure XP beads (Beckman Coulter, A63881) and prepared for sequencing with the Opto Plasma B Discovery Sanger Prep Kit (Berkeley Lights, 750-02041). Sanger sequencing was employed to determine the nucleotide sequence of the amplicons. Analysis of the VH, VL and complementarity-determining region 3 (CDR3) sequences and the percentage of somatic mutations was conducted using Geneious Prime (version 2021.0.3) and the IMGT database (<https://www.imgt.org/>). The paired VH and VL sequences of the selected mAbs were codon optimized, synthesized by Shengong Biotech, and subsequently cloned and inserted into separate mammalian expression vectors containing constant mouse IgG2a regions.

mAb expression and purification

ExpiCHO cells were cultured to a density of approximately 8×10^6 cells/mL to 1×10^7 cells/mL with a viability rate greater than 98%. The vectors were subsequently transfected into 2×10^8 ExpiCHO cells in equal volumes of Electroporation Buffer Part A and Electroporation Buffer Part B (Celetrix, 1228), and the cells were incubated at 37°C in 7% CO₂. On the first day after transfection (18–22 hours later), 10% MetaCell CHO TransFeed (Cellplus Bio, L1008) and 0.7% MetaCell Tier Enhancer (Cellplus Bio, L1009) were added to the cell culture media. After a 5-day incubation period, samples with viable cell densities greater than 50% and cell viability rates greater than 60% were collected, and the supernatants were subjected to purification using Pierce™ centrifuge columns (Thermo Scientific™, 89898). The bound mAbs were washed with buffer (5 times the sample volume) containing 100 mM Pro-Ac (pH 3.5). After washing, the pH of each sample was adjusted to 5.0 with 0.5 M Arg. The samples were then added to 50 kDa MWCO membrane centrifugal filter units (Millipore, UFC905008) for concentration. The samples were subsequently centrifuged at $3500 \times g$ for 3 minutes and then filtered through a 0.22 µm filter (Millipore, GSWP04700). The yield of the purified mAbs was determined using a BCA protein concentration determination kit (Beyotime, P0012), and the purity of the mAbs was confirmed via SDS-PAGE. The mAbs were stored at –80°C.

ELISA

First, 0.4 µg/well recombinant Omp38 or 1×10^7 colony forming units (CFUs)/well *A. baumannii* was added to 96-well ELISA plates (LABSELECT, 31111) for incubation overnight at 4°C. The plates were washed three times with PBS-Tween 20 (0.05%) (Sigma-Aldrich, P3563), blocked with 2% FBS (Gibco, A5669701) in PBS for 1 hour, and washed

three more times. Different dilutions of the recombinant mAbs or isotype control mAbs were then added for incubation at 37°C for 1 hour. After three washes, the plates were incubated with HRP-conjugated goat anti-mouse IgG (H + L) (AB Clonal, AS003) at 37°C for 1 hour. The substrate TMB (Beyotime, P0209) was then added, and the mixture was allowed to react in the dark for color development. The reaction was stopped by the addition of 1 N hydrochloric acid, and the absorbance was measured at 450 nm. The EC₅₀ was determined by fitting a non-linear regression model (four parameters).

Serum from infected mice was collected and stored at –80°C until cytokine analysis. The levels of cytokines, including interleukin-6 (IL-6), interleukin-10 (IL-10) and tumor necrosis factor alpha (TNF-α), were measured using ELISA kits (Dakewe, 1210603, 1211003 and 1217203) according to the manufacturer's instructions. Finally, the absorbance was measured at 450 nm using a microplate reader (Thermo Fisher, USA) [33].

A. baumannii adherence assay

The *A. baumannii* adherence assay was conducted according to the protocol outlined in previous studies [11,34]. A549 cells were seeded at a density of 2.0×10^5 cells/well (~100% confluence) in a 24-well plate. *A. baumannii* ATCC 17978 was cultured overnight in 10 mL of Luria – Bertani (LB) medium at 37°C with moderate shaking at 175 rpm. The bacterial suspensions were washed with PBS and adjusted to approximately 1.0×10^9 CFU/mL. After the A549 cells adhered to the wall, the complete Ham's F-12 K (Kaighn's) medium was replaced with culture medium containing inactivated FBS (56°C for 30 minutes) for preincubation at 37°C for 30 minutes to eliminate the influence of complement. The cells were subsequently infected with live *A. baumannii* strain ATCC 17978 at a multiplicity of infection (MOI) of 1:100. Then, the mAb or isotype control was added. Infected cells were incubated at 37°C with 5% CO₂ for 90 minutes. To quantify the adherent bacteria, external nonadherent bacteria were removed by washing the cells four times with PBS followed by disruption by the addition of 100 µL of Triton X-100 (1% in PBS) per well [11]. The number of adherent bacteria was then verified via the serial dilution method.

A. baumannii internalization assay

The *A. baumannii* internalization assay was conducted according to the protocol outlined in a previous study [11]. A549 cells were seeded at a density of 2.0×10^5 cells/well (approximately 100% confluence) in 24-well tissue culture plates. After the A549 cells adhered to the wall, the complete Ham's F-12 K

(Kaighn's) medium was replaced with culture medium containing inactivated FBS (56°C for 30 minutes) for preincubation at 37°C for 30 minutes to eliminate the influence of complement. The cells were subsequently infected with the live *A. baumannii* strain ATCC 17978 at an MOI of 1:100. Then, the mAb or isotype control was added. Gentamicin (100 µg/mL) was added to the culture medium to eliminate extracellular bacteria. After 2 hours of incubation, the culture medium was replaced with new medium containing 10 µg/mL gentamicin. The cells were incubated for an additional 22 hours before being lysed with 100 µL of Triton X-100 (1% in PBS) per well [11]. The number of bacteria was determined via the serial dilution method. The intracellular proliferation rate (Ipro) was calculated as the ratio of the number of viable intracellular bacteria present at 24 hours to that present at 2 hours postinfection [35–37].

Biofilm inhibition assay

A biofilm inhibition assay was conducted according to the protocol outlined in a previous study [11]. *A. baumannii* ATCC 17978 was cultured overnight in 10 mL of LB medium at 37°C with moderate shaking at 175 rpm. The bacterial suspensions were washed with PBS and adjusted to approximately 1.0×10^7 CFU/mL. A total of 180 µL of bacterial mixture and 20 µL of mAb were added to each well of a 96-well polystyrene plate. The edges of the 96-well plate were sealed with film, and the plate was incubated for 26 hours at 37°C. The formed biofilm was then fixed by treatment with 120 µL of methanol for 20 minutes. The bacterial mixture was carefully extracted, and the 96-well plate was washed twice with deionized water and air dried for 4 hours. Then, 150 µL of 0.1% crystal violet was added, and the samples were stained for 30 minutes. After removing the crystal violet solution, the samples were thoroughly washed with physiological saline until the solution was colorless and then air dried overnight. Subsequently, 120 µL of 95% ethanol was added, and the samples were incubated for 30 minutes at room temperature (RT) to loosen the biofilm. Finally, the absorbance at 600 nm was measured using a microplate reader.

Opsonophagocytosis Assay

Opsonophagocytosis Assay was conducted according to the protocol outlined in previous studies [38,39]. *A. baumannii* LAC-4 was cultured overnight in LB medium at 37°C. RAW 264.7 cells were cultured at 37°C in 5% CO₂ to a density of 3×10^5 /mL in a 96-well plate. The RAW 264.7 cells were then activated by 10 hours of exposure to the TLR2 agonist palmitoyl-2-cysteine-serine-lysine-4 (Pam₂CSK₄) (100 ng/

mL) [40]. The complete medium was replaced with culture medium containing inactivated FBS (56°C for 30 minutes) to eliminate the influence of complement. Subsequently, the RAW 264.7 cells were cocultured with *A. baumannii* LAC-4 at different MOIs (1:3, 1:30, 1:300, and 1:3000). Then, the mAb or isotype control was added to the 96-well plate. After 5 hours of incubation with gentle shaking, the presence of bacteria in the supernatant was verified via the serial dilution method.

Mouse models

C57BL/6 mice were anesthetized via intraperitoneal injection of pentobarbital sodium at a dose of 50 mg/kg. The mice were subsequently challenged with either 1.4×10^7 (lethal dose) or 1×10^6 (sublethal dose) CFU of LAC-4 in 20 µL of PBS through noninvasive intratracheal inoculation as previously described [41,42] and then immediately treated intravenously with mAbs. The LAC-4 dose was verified via the serial dilution method. To monitor the survival rate of the mice with lethal *A. baumannii* infection, 8 mice in each group were euthanized by cervical dislocation at 72 hours postinfection. To determine the toxicity of mAb C3, 5 mice in each group were euthanized by cervical dislocation 72 hours after C3 injection. To investigate the bacterial load and pathology of lethal *A. baumannii* infection, 5 mice in each group were euthanized by cervical dislocation at 24 hours postinfection. To evaluate the bacterial load, pathology, immune cell infiltration and cytokine production resulting from sublethal *A. baumannii* infection, 5 mice in each group were euthanized by cervical dislocation at 24 hours postinfection.

Histopathology

Formalin-fixed and paraffin-embedded (FFPE) tissues were sectioned into 5 mm thick slices and stained with hematoxylin and eosin (H&E) following the manufacturer's instructions (Solarbio, G1120). Images were acquired using a bright field microscope (Nikon TE2000). A previously described scoring system assessing (a) neutrophil infiltration, (b) edema, (c) disorganization of the lung parenchyma and (d) hemorrhage was used to determine the degree of acute lung injury (ALI) in a double-blinded manner [43,44]. Higher scores indicate more severe lung abnormalities, as follows: 0 = normal, 1 = light, 2 = moderate, 3 = severe, and 4 = very severe. The scores from each of the four categories were combined to provide a total lung injury score (maximum score, 16) [43,44]. Kidney and liver toxicity severity were also scored as follows: 0 = no abnormalities; 1 = renal tubulointerstitial lesions/liver lobular destruction/inflammatory cell infiltration/liver lobular necrosis

area <5%; 2 = 5%–25%; 3 = 25%–75%; and 4 = >75% [45]. Three randomly selected fields of each sample were scored, and the average score was calculated.

Cell viability determination using the cell counting kit-8 (CCK-8) assay

The impact of the mAb on cell viability was determined by the CCK-8 assay. A549 cells, RAW264.7 cells and 293 T cells were seeded into 96-well plates in 100 μ L of complete medium and cultured at 37°C with 5% CO₂. After the cells adhered to the wall, the mAb was added to the culture medium. At the end of each experiment, 10 μ L of CCK-8 reagent (Beyotime, C0038) was added to each well, and the cells were cultured for an additional 1 hour at 37°C. Then, the optical density at 450 nm was measured using a microplate reader (Thermo Fisher, USA). Cell viability was determined using the following formula: Cell viability (%) = $[A(\text{dosing}) - A(\text{blank})] / [A(0 \text{ dosing}) - A(\text{blank})] \times 100\%$, where A (dosing) is the absorbance of the well containing cells, CCK-8 reagent, and the mAb; A (blank) is the absorbance of the wells containing culture media and CCK-8 solution but no cells; and A (0 dosing) is the absorbance of the wells containing cells and CCK-8 reagent but no mAb.

Flow cytometry

The lungs of the animals were cut into small pieces and digested in a standard test tube with 5 mL of digestion buffer (0.5 mg/mL collagenase and 20 mg/mL DNase diluted in RPMI medium) for 45 minutes. The cell suspension was then passed through a 70 μ m pore size cell strainer, and the remaining cells were lysed with ACK buffer (Invitrogen, A1049201). After digestion, the cells were blocked with mouse BD FC Block (BD Pharmingen, 553141) and then stained with fluorescently labeled mAbs as follows: CD4-fluorescein isothiocyanate (FITC) (clone GK1.5); CD45-PerCP-Cyanine 5.5 (clone HI30); F4/80-phycoerythrin (PE)-Cyanine 7 (clone BM8); LY6G-allophycocyanin (APC) (clone 1A8-Ly6 g); L/D APC-CY7 (LIVE/DEAD™ Fixable Near-IR Dead Cell Stain Kit, Invitrogen); and CD8-AmCyan (clone SK1). The cells were stained with antibodies (1:200) at 4°C for 30 minutes. Data were acquired with a BD FACSCanto II cell analyzer and analyzed with FlowJo software (Tree Star, Ashland, OR).

Flow cytometry was conducted following the instructions of the Annexin V Apoptosis Detection Kit (Invitrogen, 88-8006-72) to determine the impact of the mAb on apoptosis. A549 cells, RAW264.7 cells and 293 T cells were seeded into 24-well plates in 1 mL of complete medium and cultured at 37°C with 5% CO₂. After treatment with 50 μ g/mL mAb C3 for 5 hours, the cells were gently digested with

trypsin and washed once with PBS and once with 1 \times binding buffer. The cells were resuspended in 1 \times binding buffer at a density of 1–5 $\times 10^6$ /mL, and 5 μ L of fluorochrome-conjugated Annexin V was added to 100 μ L of cell suspension. After incubation for 10–15 minutes at RT, the cells were washed with 1 \times binding buffer and resuspended in 200 μ L of 1 \times binding buffer. 7-Amino-actinomycin (7-AAD; 5 μ L) viability staining solution (Invitrogen, 00-6993-50) was added, and the samples were analyzed by flow cytometry.

Identification of the sequence types (STs) of *A. baumannii* strains

Multilocus sequence typing (MLST) was performed using the scheme developed by Laure Diancourt and colleagues (Pasteur scheme) to determine the STs of the *A. baumannii* strains [46]. Pasteur scheme's specific loci included 60-kDa chaperonin (cpn60), elongation factor EF-G (fusA), citrate synthase (gltA), CTP synthase (pyrG), homologous recombination factor (recA), 50S ribosomal protein L2 (rplB), and RNA polymerase subunit B (rpoB) [47,48]. The Fast-All (FASTA) sequences of 9 clinical *A. baumannii* strains were retrieved from the next-generation sequencing data and uploaded in batch sequence query mode to the *A. baumannii* MLST Database (<http://pubmlst.org/abaumannii/>) to generate allelic profiles at each of the 7 loci. The STs of 9 clinical *A. baumannii* strains were then determined using the Pasteur scheme.

Statistical analysis

GraphPad Prism 8.0 was used for statistical analysis. Parametric comparisons between two or more groups were performed using Student's *t* test or one-way analysis of variance (ANOVA) and Tukey's multiple comparisons test, respectively. Nonparametric comparisons between more than two groups were performed using the nonparametric Kruskal-Wallis test and Dunn's post hoc test. Survival rates among groups were determined by the log-rank (Mantel-Cox) test. The data are presented as the means \pm standard errors of the means (SEMs). A significance threshold of $P < 0.05$ was applied.

Results

A. baumannii OMPs can induce the production of high titers of specific polyclonal IgG antibodies

OMPs from *A. baumannii* were successfully isolated, and SDS-PAGE revealed a single predominant band corresponding to the OMPs at approximately 38 kDa, which is consistent with previous studies [49]

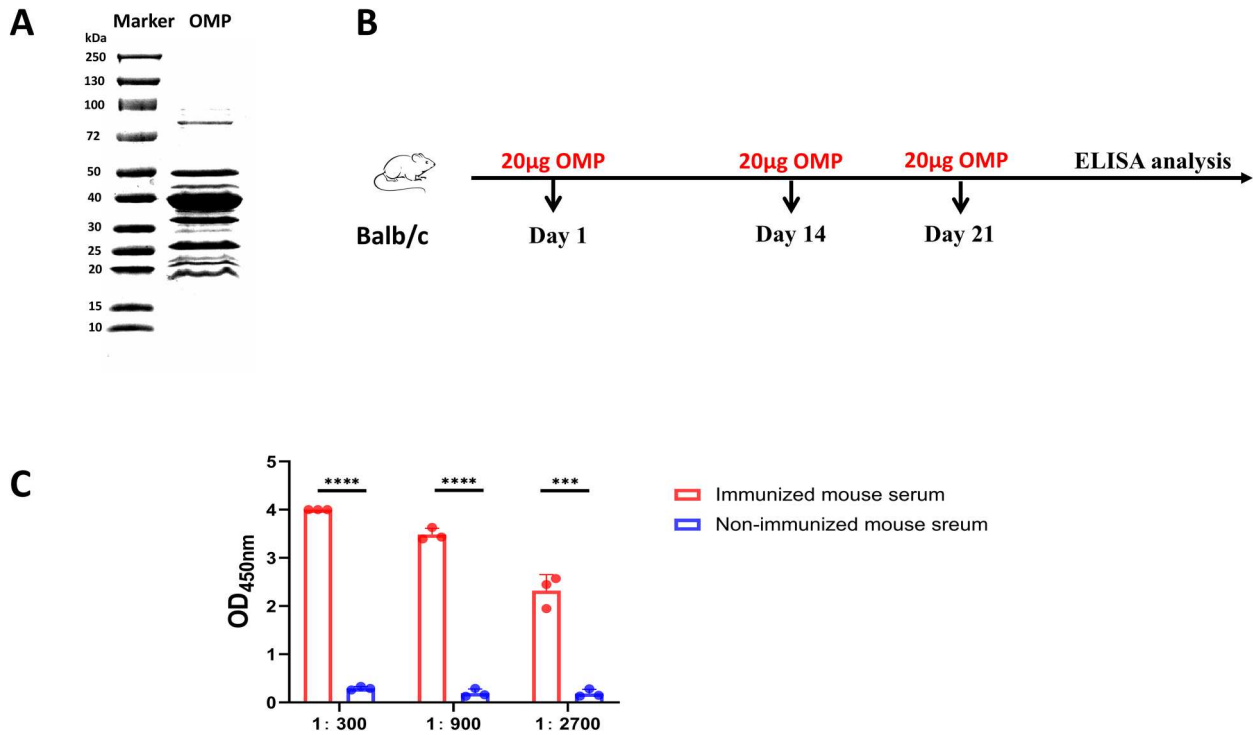


Figure 1. A specific IgG response is efficiently induced in mice via the use of purified OMPs. (A) SDS-PAGE confirmed the presence of OMPs isolated from *A. baumannii*. (B) Schematic of BALB/c mouse immunization. The first dose of OMPs mixed with 50 μ L of QuickAntibody Mouse3W for BALB/c mouse immunization was injected into the calf muscles of the leg, followed by two more doses on days 14 and 21. ELISA confirmed the presence of anti-OMP antibodies after the third injection. Each mouse received a final booster of OMPs intraperitoneally three days prior to Beacon system testing. (C) The titer of OMP-specific polyclonal IgG antibodies at serial dilutions of 1:300, 1:900 and 1:2700 in the serum obtained from immunized mice was assessed via ELISA. The values represent the means of triplicate technical replicate experiments, with SEMs indicated in the graph, and the significant differences in OMP-specific antibody levels compared with those in the non-immunized group are shown. ***, $P < 0.001$; ****, $P < 0.0001$; unpaired Student's t test.

(Figure 1(A)). Compared with that in the nonimmunized group, the OMP-specific polyclonal IgG antibody titer after three OMP immunizations was greater in the OMP-immunized group (Figure 1(B,C)).

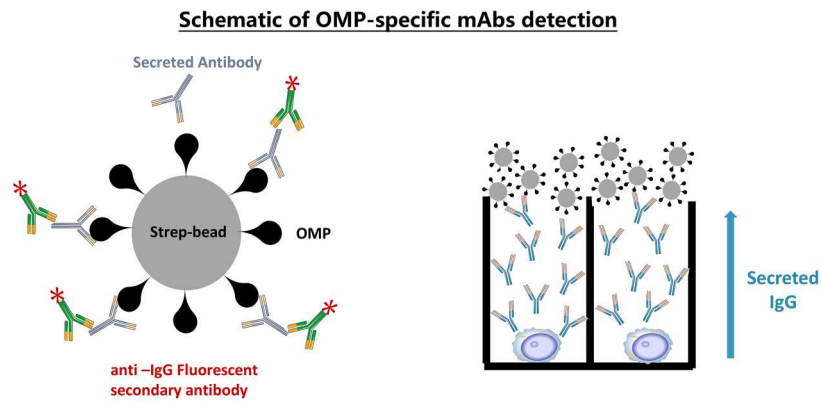
High-throughput analysis of the single B-cell secretion of OMP-specific mAbs

Biotinylated OMPs (black) and streptavidin-conjugated assay beads (gray) were loaded into the channel above the NanoPens. Single B-cells secreted antibodies (purple and Y-shaped) into the NanoPens, and the antibodies that bound to the OMPs were detected via fluorescent anti-mouse IgG secondary antibodies (green with red asterisks) (Figure 2(A)). Thus, the reactive antibodies that diffused out of a pen were observed as a bloom of fluorescence (Figure 2(B)). Three days after the final booster, plasma cells from bone marrow, lymph nodes, and spleen were collected from immunized mice. The plasma cells were enriched and loaded into the Berkeley Lights Beacon optofluidic instrument in supportive medium for cell survival. High-throughput single-cell analysis confirmed the successful loading of 10,661 cells into individual NanoPens on the device chip (Figure S1A). In addition, IgG beads were loaded into individual NanoPens on the chip to quantify the number of antibody-

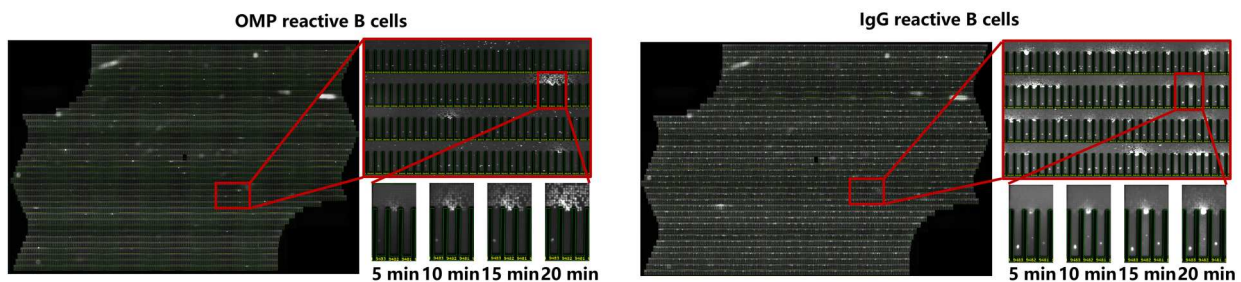
secreting plasma cells (Figure 2(B), right panel). Among the 10,661 cells loaded into NanoPens, 47 were identified as producing OMP-specific antibodies (Figure S1A and Figure 2(B), left panel). Then, PCR was performed to amplify both light and heavy chain sequences of the 47 single cells derived from the Beacon platform (Figure S1B). Despite encountering challenges with cDNA amplification of the VH or VL genes in exported cells, we ultimately obtained information for the genes encoding both the VH and VL regions from 24 candidates (Figure S1B).

Using the IMGT database, we conducted a complementarity-determining region (CDR) analysis and identified antibodies, such as B1, F4, H3, F1, F3, D4, D6, and A6, with highly similar sequences in the CDRs of both VH and VL (Figure 2(C) and Figure S1C). Considering the similarity in the VH and VL CDRs among the different mAbs, 9 antibodies with different VH and VL CDRs were selected for further analysis, including F4, A2, B4, C3, G1, G4, H4, G3, and E6 (Figure 2(C)). We subsequently analyzed the variable region identities and germline characteristics of the VH and VL for these antibodies. The VHs of F4, A2, B4, and C3 belong to the VH1-18 family, whereas their light chains belong to the VK14-126 family (Figure 2(C)). In contrast, the VHs of G1 and E6 belong to the VH1-18-26 and VH5-9-4 families,

A



B



C

mAb	VDJ Heavy	V region identity(%)	VH CDR1	VH CDR2	VH CDR3
F4	VH1-18/JH4/DH3-1	94.10	GYTFTAYTMH	GINPKNGGTS	GAYY
A2	VH1-18/JH4/DH3-1	95.14	GYTFTEYTMH	GINPKNGGIS	GAYY
B4	VH1-18/JH4/DH3-1	94.79	GYTFTEYTMH	GINPKNGGFS	GAYY
C3	VH1-18/JH4/DH3-1	95.83	GYTITEYTMH	GINPNNGGTS	GAYY
G1	VH1-18-26/JH2/DH1-2	95.14	GYTFTDYNVH	FIYPNNGLTG	GATTSAFDY
mAb	VJ Light	V region identity(%)	VL CDR1	VL CDR2	VL CDR3
F4	VK14-126/JK5	97.85	KASQDIKSYLT	YATRLAD	LQHGESPLT
A2	VK14-126/JK5	97.49	KASQDIKSYLT	YATNLAD	LQHGESPLT
B4	VK14-126/JK5	97.85	KASQDIKSYLT	FATSLAD	LQHGESPLT
C3	VK14-126/JK5	98.21	KASQDIKSYLT	YARTLAD	LQHGESPLT
G1	VK1-117/JK1	99.32	RSSQRIVHSNGNTYLE	KVSNRFS	FQGSHPVWT
mAb	VDJ Heavy	V region identity(%)	VH CDR1	VH CDR2	VH CDR3
G4	VH5-9-4/JH3/DH1-2	97.57	GFTFSSYAMS	EISSGGTYTY	EGDGYVWFY
H4	VH1-42-1/JH2/DH1-3	90.62	GYSFDGYGMN	LIIPYNGRTN	GNYGSSPDY
G3	VH1-42-1/JH2/DH1-1	89.93	GYSFDGYAIK	LIIPYNGRTS	GSYGSSPDY
E6	VH1-18-26/JH2/DH2-10	95.49	GYTITDYNMH	YISPYNGGSG	DLVWSSHFDY
mAb	VJ Light	V region identity(%)	VL CDR1	VL CDR2	VL CDR3
G4	VK12-41/JK5	99.28	RASGNIHNYLA	NAKTLAD	QHFLTTPRALT
H4	VK9-124/JK4	98.92	RASQEISGYLS	AASTLDS	LQYDYPFT
G3	VK9-124/JK4	98.92	RASQEISGYLS	AASTLDS	LQYDYPFT
E6	VK19-93/JK1	97.85	KASQDINKYIA	YTSTLQP	LQYDNLWT

Figure 2. Acquisition of mAbs secreted by single OMP-reactive B cells. (A) Schematic of OMP-specific mAb detection. Left: Biotinylated OMPs (black) with streptavidin conjugated to polystyrene beads (gray). Antibodies (purple, Y-shaped) secreted by single B cells were loaded into a single NanoPen, and OMP-specific antibodies were detected with a fluorescent anti-mouse IgG secondary antibody (green with red asterisk). Right: Schematic of the antigen-specific reactivities of antibodies secreted by a single B-cell in the pen and the fluorescent beads in the channel. (B) An 11k chip loaded with OMP-conjugated beads (left panel) or IgG beads (right panel), with a magnified view of a section to highlight the binding between the antibodies and beads over pens with OMP-reactive B cells or IgG-reactive B cells. (C) Germline, CDR1, CDR2, and CDR3 nucleotide sequences and variable region identities of the heavy or light chains of the recombinant mAbs were analyzed using the IMGT database. Strep-bead: streptavidin-conjugated assay beads.

respectively, and their VLs belong to the VK1-117 and VK19-93 families, respectively (Figure 2(C)). The VH of antibody G4 is from the VH5-9-4 family, while its VL is from the VK12-41 family (Figure 2(C)). The VHs of H4 and G3 belong to the VH1-42-1 family, whereas their VLs belong to the VK9-124 family (Figure 2(C)). Moreover, except the G3 VH (89.93%), the VHs presented more than 90% identity in their variable regions with respect to their respective germline genes (Figure 2(C)). Finally, we expressed and purified mAbs containing the IgG2a constant region (IgG2a mAbs) and the variable region of the above selected antibodies in CHO cells (Figure S2).

Binding activity of Omp38-specific mAbs to the LAC-4 *A. baumannii* strain

As one of the major or most studied *A. baumannii* OMPs, Omp38 has been reported to play an important role in bacterial adherence to and invasion of host cells [1,11,27]. Recombinant Omp38 was expressed and purified for further investigation of the specificity of the above mAbs (Figure 3(A)). ELISAs confirmed the high binding affinity of the mAbs, including F4, G1, B4, G4, C3, and A2, to Omp38 (Figure 3(B)). However, H4, G3, and E6 did not bind to Omp38, indicating their likelihood of binding to other OMPs (Figure 3(B)). Next, the binding activities of the mAbs with the highly virulent *A. baumannii* strain LAC-4 (ST10 subtype) was examined [47]. All of the above Omp38-specific mAbs showed affinity for LAC-4, with EC50 values ranging from 1.08 µg/mL to 37.39 µg/mL (Figure 3(C)).

Binding activity of Omp38-specific mAbs to clinical *A. baumannii* strains

Then, we collected 9 clinical *A. baumannii* strains and identified their STs to investigate the abilities of the mAbs to bind to strains other than LAC-4. Notably, strains 3, 4, 5, 7, and 9 belonged to ST2, whereas strains 1, 2, 6, and 8 were identified as belonging to ST193, ST205, ST63, and ST584, respectively (Figure 4(A)). ELISA demonstrated that mAbs F4, A2, C3, G1, G4, and B4 demonstrated binding to the 9 clinical *A. baumannii* strains (Figure 4(B)).

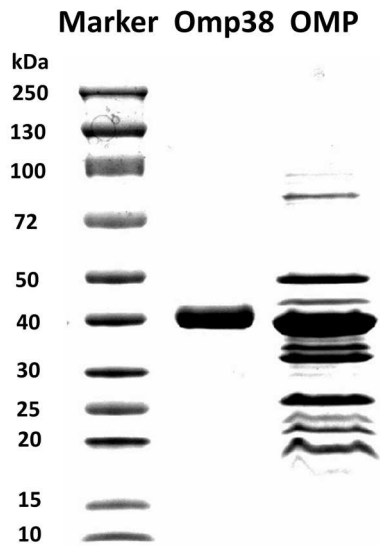
Omp38-specific mAbs confer protection against lethal *A. baumannii* infection in mice

To assess the protective efficacy of the mAbs against infection by the highly virulent *A. baumannii* strain LAC-4 in mice, animals were intratracheally inoculated with a lethal dose of LAC-4 and promptly treated with Omp38-specific mAbs. Then, the survival rate was monitored for 72 hours postinfection (Figure 5(A)). Notably, four out of the six candidate mAbs (F4, A2, C3, and G4) protected against LAC-4

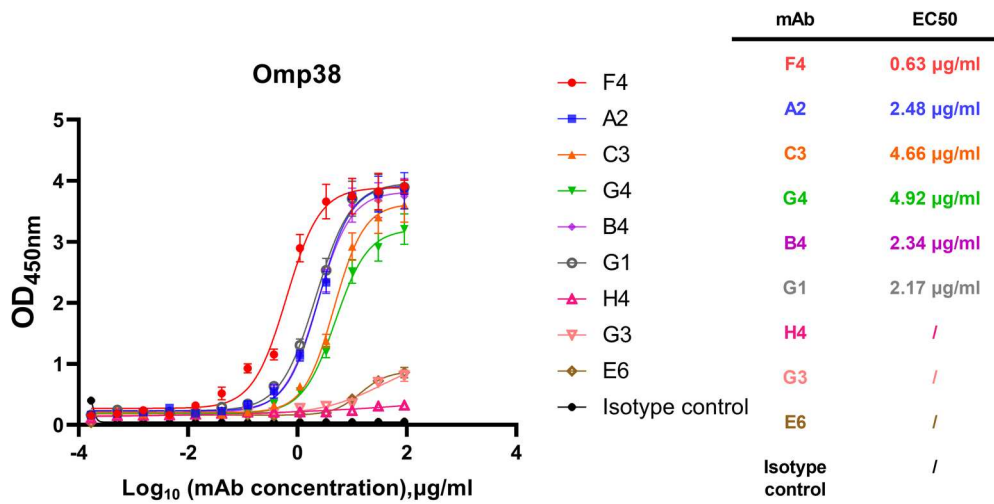
infection, with 50% protection in 4 out of 8 mice, 75% protection in 6 out of 8 mice, and 62.5% protection in 5 out of 8 mice (Figure 5(B)). In recent years, antibody cocktail therapy has emerged as a more effective treatment option than single antibody therapy because of its advantages, such as an increase in the diversity and complexity of the antibodies [50]. Notably, a two-antibody cocktail (C3 + G4) at a final dosage of 15 mg/kg per mouse, that is, 7.5 mg/kg per antibody, conferred 100% protection to 8 mice. The three-antibody cocktails C3 + G4 + A2 and C3 + G4 + F4 at a final dosage of 15 mg/kg (5 mg/kg per antibody) conferred 87.5% protection in 6 out of 8 mice and 75% protection in 6 out of 8 mice. However, the survival curve of the mice treated with the four-antibody cocktail (C3 + G4 + A2 + F4) at a final dosage of 15 mg/kg (3.75 mg/kg per antibody) did not significantly differ from that of the mice treated with the isotype control (Figure 5(C)). Since *A. baumannii* causes systemic bloodstream infections [8], we investigated the bacterial load in the blood, lungs and kidneys, as well as pathological damage to the mouse organs (Figure 5(D)). At 24 hours postinfection, the mice treated with C3 presented 24-fold, 30-fold, 38-fold and 206-fold reductions in bacterial load in the blood, liver, kidney and lung, respectively (Figure 5(E)). To assess the impact of mAb C3 on mitigating pathological injury, the lungs, livers and kidneys were collected, and H&E staining revealed lower lung injury, liver severity and kidney severity scores in the C3-treated group than in the isotype control group (Figure 5(F)).

The *in vitro* and *in vivo* safety of mAb C3 was subsequently confirmed. Flow cytometry analysis revealed that C3 did not influence the percentage of late apoptotic (Annexin V⁺7-AAD⁺) cells or early apoptotic (Annexin V⁺7-AAD⁻) cells (Figure S3A). A CCK-8 assay demonstrated that mAb C3 did not influence the viability of various cells (293 T cells, RAW264.7 cells or A549 cells) after treatment with 50 µg/mL for different durations (Figure S3B, left) or treatment with different concentrations of C3 for 5 hours (Figure S3B, right). For toxicity analysis, the mice were treated with 15 mg/kg C3 or the same volume of PBS. At 72 hours postinjection, serum was collected to detect serum biochemical indicators, including total protein (TP), albumin (ALB), alanine aminotransferase (ALT), aspartate aminotransferase (AST), total cholesterol (TC), alkaline phosphatase (ALP), albumin/globulin (A/G), direct bilirubin (TBIL), urea (UREA), serum creatinine (SCR), glucose (GLU), creatine kinase (CK) and triglyceride (TG) levels. In addition, the liver, kidney, intestine, lung, spine, brain, spleen and heart were collected to detect pathological changes. The results revealed that after treatment with C3, there were no changes in the biochemical indicators or pathological damage to the organs (Figure S3C and Figure S3D).

A



B



C

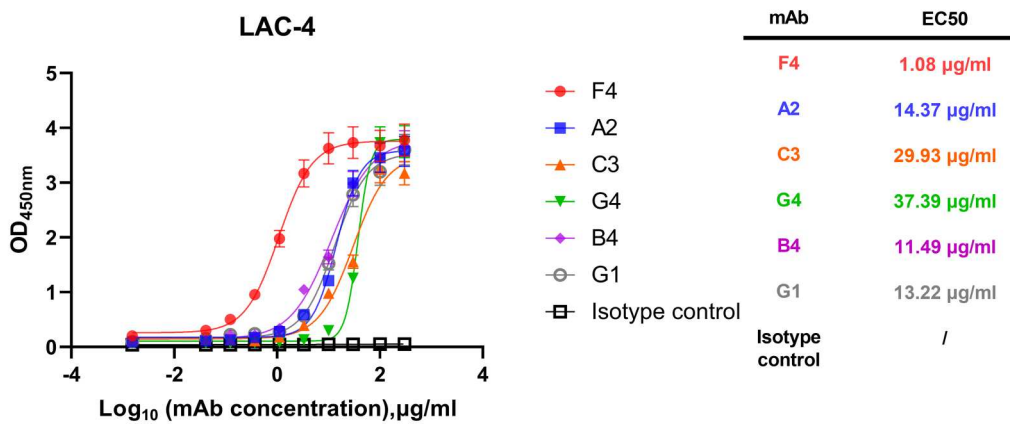


Figure 3. Binding capacity of mAbs to Omp38 and LAC-4. (A) SDS-PAGE confirmed the expression of recombinant Omp38. To facilitate purification by affinity chromatography, 1 additional methionine and 6 histidine tags were added to the recombinant Omp38, resulting in an Omp38 that is 972.05 Da larger than the native state. (B) ELISA assessment of the reactivities of the mAbs to Omp38. (C) Binding capacity of mAbs to *A. baumannii* strain LAC-4. Curves were fitted using 4-parameter nonlinear regression. The means \pm SEMs are shown, with $n = 3$ technical replicates for (B) and (C).

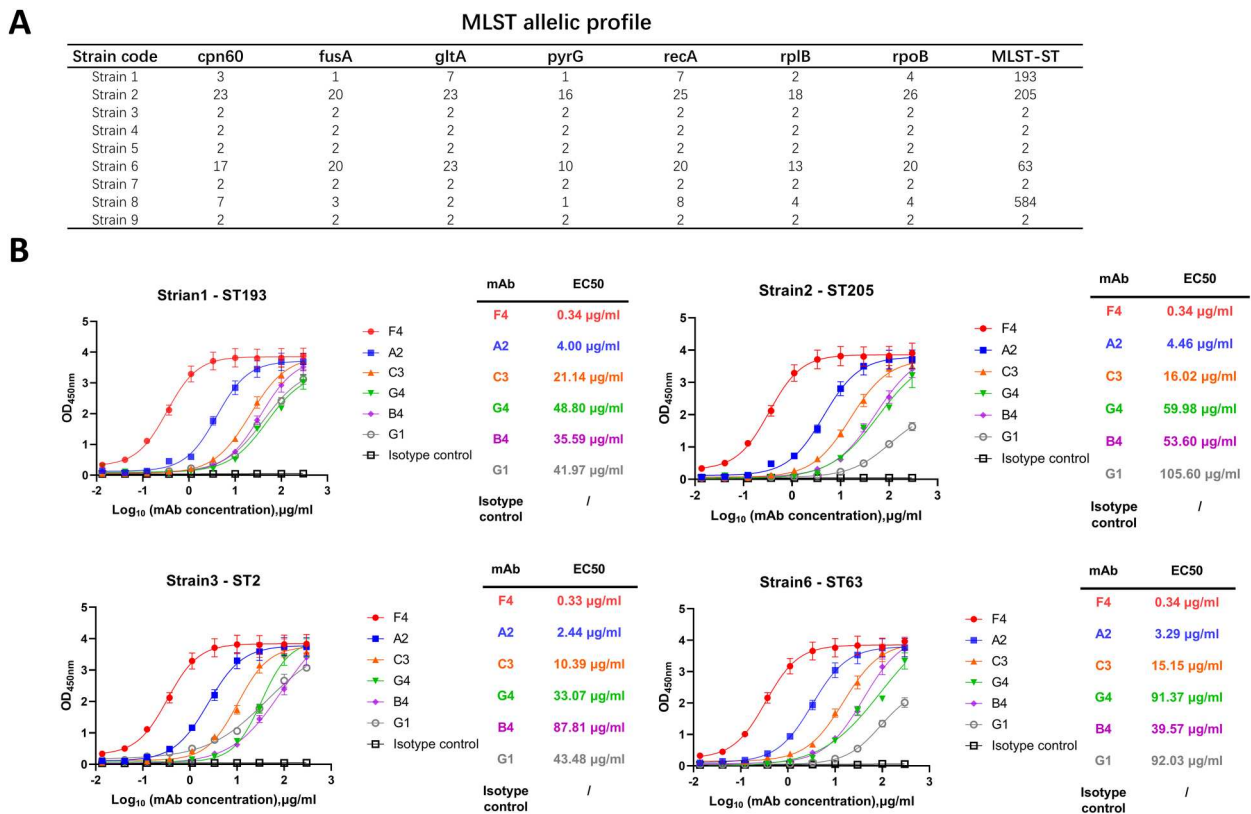


Figure 4. Binding capacity of mAbs to clinical *A. baumannii* strains. (A) Identification of the STs of 9 clinical strains. (B) Binding activity of F4, A2, C3, G1, B4, and G4 to clinical *A. baumannii* strains. The means \pm SEMs are shown, with $n = 3$ technical replicates.

Omp38-specific mAbs provide protection against sublethal *A. baumannii* infection in mice

The effectiveness of the mAbs was also evaluated in an aspiration pneumonia model, which closely mimics the typical clinical manifestations of *A. baumannii* infection and is another clinically relevant *in vivo* model (Figure 6(A)). Importantly, at 24 hours postinfection, the 5 mice treated with C3 or G4 presented 2885-fold or 857-fold reductions in the lung bacterial load of LAC-4, respectively, compared with that in the mice treated with the isotype control mAb, whereas treatment with F4 or A2 resulted in an approximately 100-fold reduction (Figure 6(B)). An increase in the severity of inflammation with leukocyte infiltration and a cytokine burst were observed after *A. baumannii* infection [41,51]. Then, to assess the potential anti-inflammatory effects of the Omp38-specific mAbs, their impact on intrapulmonary cytokine concentrations was investigated. Treatment with Omp38-specific mAbs led to a significant reduction in the levels of proinflammatory cytokines (IL-6 and TNF- α) and the anti-inflammatory cytokine IL-10, which correlated with reduced bacterial loads (Figure 6(C)). Flow cytometry analysis further revealed reduced infiltration of immune cells, including total leukocytes (CD45⁺ cells), neutrophils (CD45⁺ Ly6G⁺ cells), mononuclear macrophages/monocytes (CD45⁺ F4/80⁺ cells), and CD4⁺ T cells (CD45⁺ CD4⁺ cells), into the lungs of

the mAb-treated mice (Figure 6(D) and Figure S4). To assess the potential of using the mAbs to mitigate lung pathology, lungs were collected 24 hours postinfection for H&E staining. The results showed that Omp38-specific mAbs reduced inflammatory cell infiltration and alveolar wall thickening, ultimately mitigating damage to the lung tissue structure (Figure 6(E)). Lung injury was scored 24 hours postinfection, and mice treated with Omp38-specific mAbs presented lower scores than did the mice treated with the isotype controls (Figure 6(E)), suggesting that Omp38-specific mAbs reduce damage to the lung tissue structure.

Protective mechanism of Omp38-mAb C3 against *A. baumannii* infection

Epithelial cells constitute the first line of defense for immune protection in the host. *A. baumannii* biofilms promote the adherence and colonization of the bacteria on the surface of respiratory epithelial cells, resulting in intracellular proliferation and the death of host cells [11,52]. Since Omp38 has been reported to play important roles in adherence, intracellular proliferation, and biofilm formation [11,52,53], we explored the impact of C3 on the pathobiology of *A. baumannii*. Compared with the isotype control, C3 inhibited the biofilm formation, adherence and intracellular proliferation of *A. baumannii* (Figure 7(A–C)).

Antibody-dependent cellular phagocytosis (ADCP) is an immunological mechanism of elimination

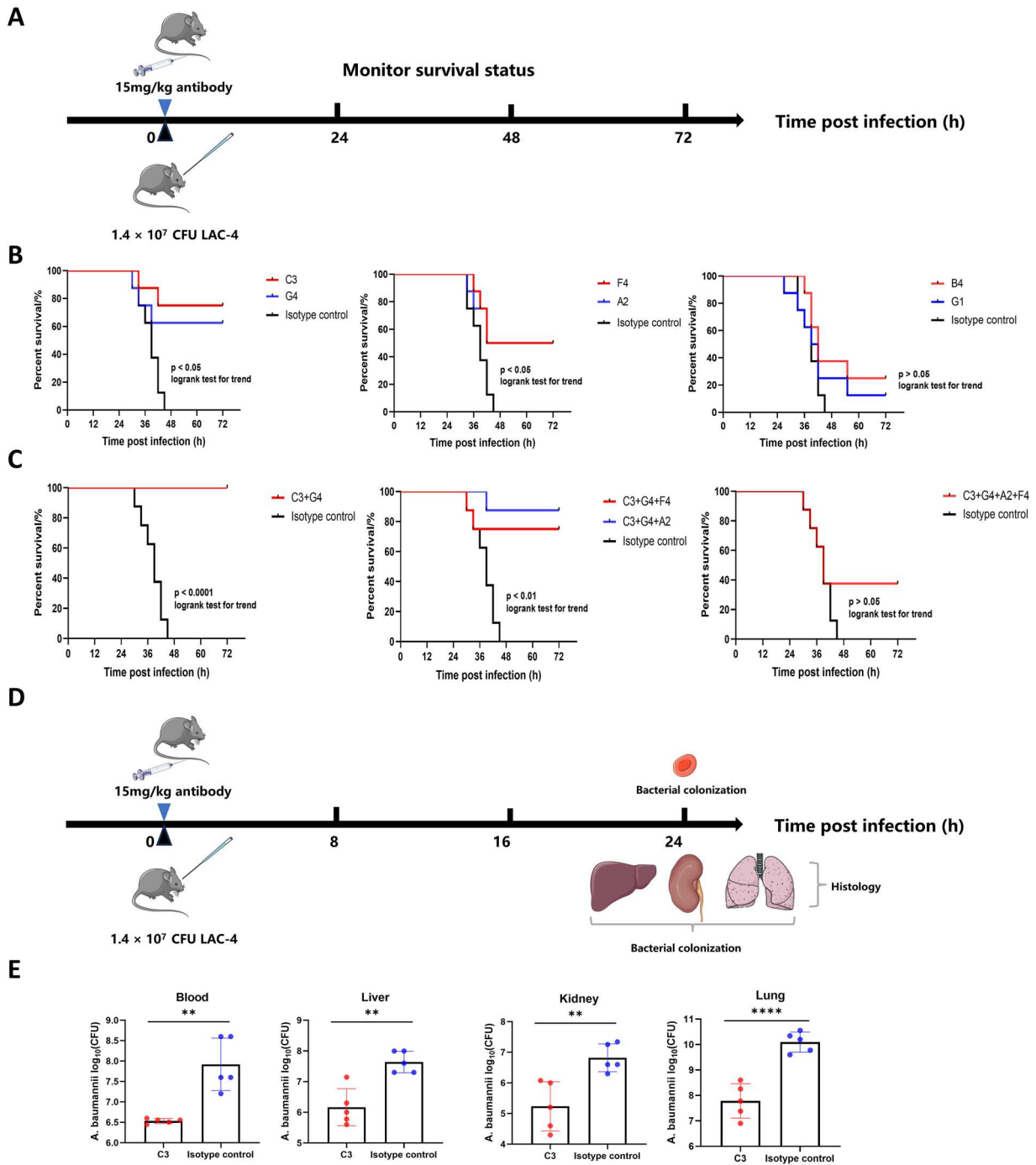


Figure 5. mAbs significantly increased the survival rate after lethal infection caused by the highly virulent *A. baumannii* LAC-4 strain. (A) Schematic of Omp38-specific mAb treatment of model mice with lethal LAC-4 infection. Eight mice were noninvasively intratracheally inoculated with a lethal dose (1.4×10^7 CFU) of LAC-4 and immediately treated with 15 mg/kg mAbs (F4, A2, C3, or G4), the isotype control mAb or a mixture of mAbs. Survival status was monitored for 72 hours after infection. (B) Kaplan-Meier survival curve of infected mice treated with a single mAb versus isotype controls ($n = 8$ in each group, biological replicates). (C) Kaplan-Meier survival curve of infected mice treated with a mixture of mAbs versus isotype controls ($n = 8$ in each group, biological replicates). (D) Schematic of mAb C3 treatment of model mice with lethal LAC-4 bloodstream infection. Five mice were noninvasively intratracheally inoculated with a lethal dose (1.4×10^7 CFU) of LAC-4 and immediately treated with 15 mg/kg mAb C3 or isotype control. Blood, liver, kidney and lung samples were collected 24 hours after infection, and H&E staining and pathological scoring were subsequently conducted. (E) The bacterial load was quantified via the serial dilution method. The results are presented as \log_{10} CFU per gram ($n = 5$ in each group, biological replicates). (F) Representative H&E staining images of the lung, liver and kidney 24 hours postinfection ($n = 5$ in each group, biological replicates). The lung injury, liver severity and kidney severity scores were assessed in a double-blinded manner ($n = 5$ in each group, biological replicates). Survival curves were compared via the log-rank (Mantel-Cox) test. Isotype data were the same among the different panels. Comparisons of bacterial loads between the groups were carried out via unpaired Student's *t* test. Comparisons of pathological scores between the groups were carried out via the Kruskal-Wallis nonparametric test and Dunn's post hoc test. The means \pm SEMs are shown. *, $P < 0.05$; **, $P < 0.01$; ****, $P < 0.0001$. Blank refers to healthy mice that were not infected. h: hours.

F

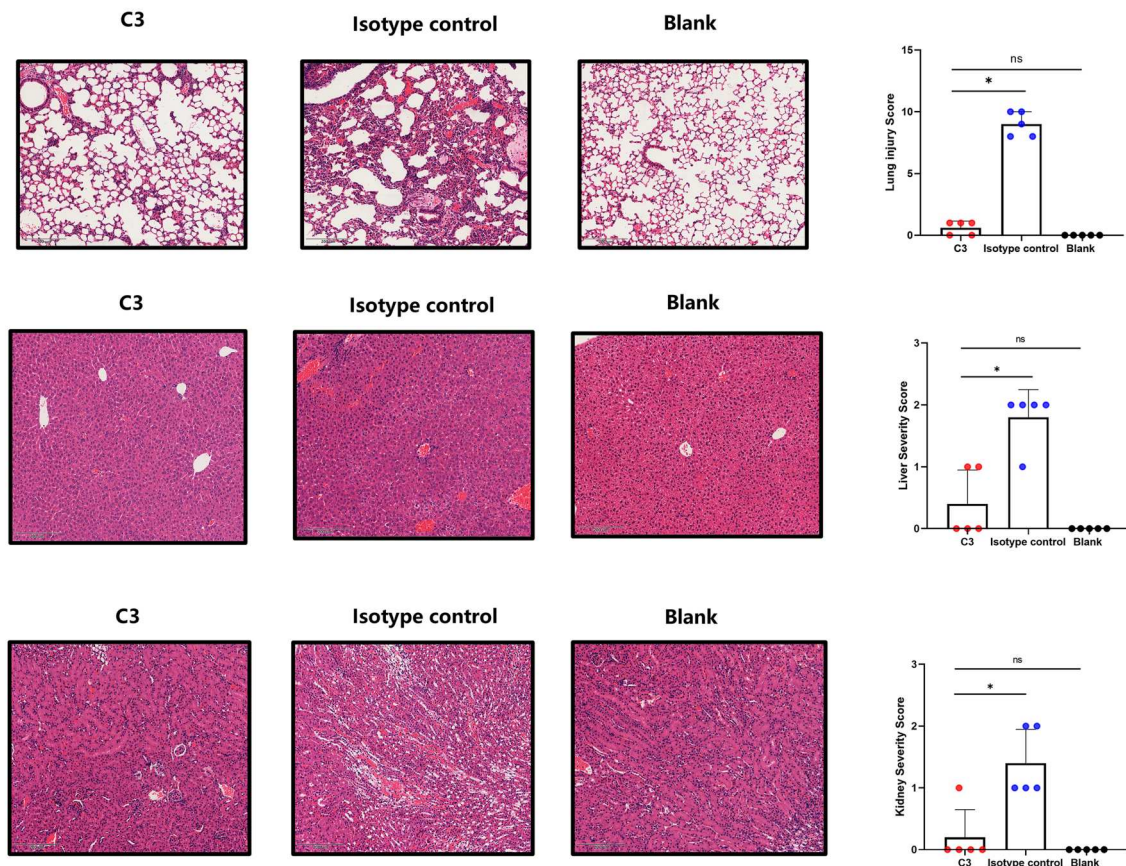


Figure 5. Continued

whereby infected cells are targeted by mAbs to promote their clearance from the body by phagocytic immune cells such as macrophages [54]. A previous study revealed that macrophages play an important role in early host defense against *A. baumannii* infection through efficient phagocytosis and killing of *A. baumannii* [55]. Therefore, we investigated the role of C3 in ADCP. Macrophage uptake of the hypervirulent *A. baumannii* strain LAC-4 increased in the presence of mAb C3 at MOIs of 3 and 30 but did not differ at MOIs 300 and 3000 (Figure 7(D)). These results confirmed the role of C3 in antibacterial sterilization via the induction of ADCP.

Analysis of the Omp38-mAb C3 binding conformation to explore the potential mechanism of the broad-spectrum binding activity of mAb C3

We chose mAb C3 for analysis of the antigen – antibody binding conformation because of its superior *in vivo* efficacy and ability to bind *A. baumannii* strains from diverse sources. Using AlphaFold 3 and GeoBiologics, the binding between mAb C3 and the *A. baumannii* reference strain from NCBI GenBank (ATG88079.1) was predicted, which suggested that C3 might bind the extracellular domain of Omp38 (Figure 8(A)). In addition, 3 loop structures in this

domain were identified (Figure 8(A,B)). The residues in the 3 loops of the various *A. baumannii* strains, including the reference strain, LAC-4, and the above 9 clinical strains, were subsequently extracted and aligned. Notably, some *A. baumannii* strains, such as strains 2 and 6, presented identical loop structures; thus, subsequent analyses of these strains were conducted together (Figure 8(C)). The 11 strains were ultimately divided into 5 groups, from which 5 binding conformations were identified on the basis of homology modeling. To explore whether the changes in the loops influence the binding affinity of C3, 10 ns of molecular dynamics simulations were performed for each complex, and CHARMM tools in Discovery Studio 2.5 were used to calculate the binding energy between C3 and different strains of *A. baumannii*. Notably, C3 exhibited similar interaction energies for the 11 strains from diverse sources (Figure 8(D)), which was consistent with the ELISA results (Figure 4(B)), indicating the broad-spectrum binding activity of C3.

The 5 binding conformations were further analyzed by structural alignment with a focus on the interactions between the 3 loop regions of the *A. baumannii* strains mentioned above and the CDR of C3. Since hydrogen bonds are, in most cases, critical for high-specificity and high-affinity antigen-antibody interactions [56,57], we used the reference strain as an

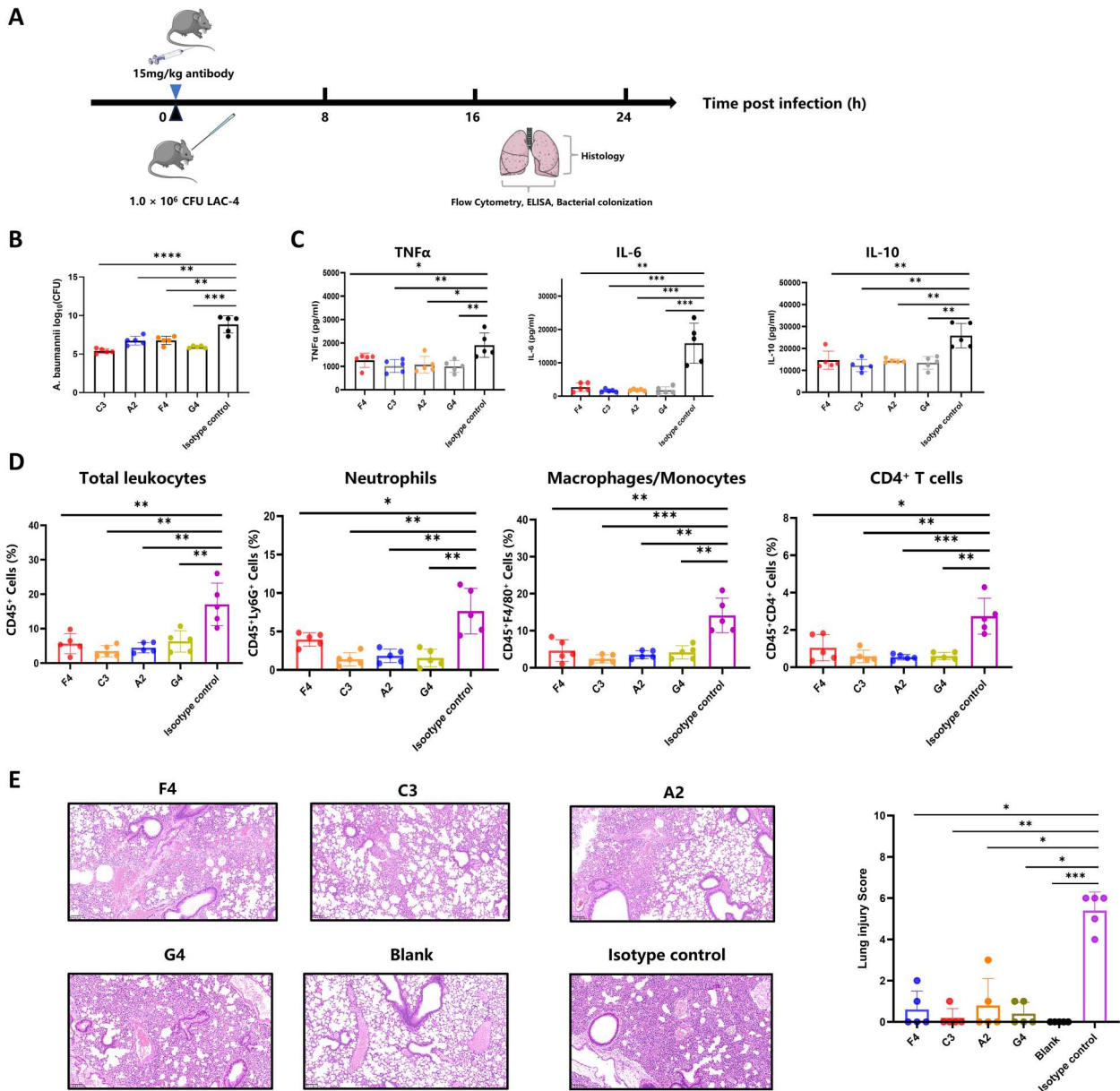


Figure 6. mAbs decreased the bacterial load, inflammatory response and degree of lung injury upon sublethal infection with the LAC-4 strain. (A) Schematic of Omp38-specific mAb treatment of model mice with sublethal LAC-4 infection. The mice were non-invasively inoculated intratracheally with a sublethal dose (1.0×10^6 CFU) of LAC-4 and then treated intravenously with F4, A2, C3, G4 or an isotype control mAb. (B) The bacterial load was quantified by the serial dilution method. The results are presented as \log_{10} CFU per gram of lung ($n = 5$ in each group, biological replicates). (C) ELISA results showing the changes in the levels of cytokines in the lungs of the isotype control and infected mice ($n = 5$ in each group, biological replicates). (D) Flow cytometry analyses showing the percentages of total leukocytes, neutrophils, macrophages/monocytes, and CD4⁺ T cells ($n = 5$ in each group, biological replicates). (E) Representative H&E-stained sections of lung tissues 24 hours postinfection and the lung injury scores ($n = 5$ in each group, biological replicates). Comparisons between the isotype control and Omp38-specific mAb-treated groups were carried out via one-way ANOVA and Tukey's multiple comparisons test. Comparisons of the lung injury scores between the groups were carried out via the Kruskal-Wallis nonparametric test and Dunn's post hoc test. The means \pm SEMs are shown. *, $P < 0.05$; **, $P < 0.01$; ***, $P < 0.001$; ****, $P < 0.0001$. Blank refers to healthy mice that were not infected. h: hours.

example and highlighted the crucial hydrogen bonds involved in the interactions between the CDRs of the light and heavy chains and loop regions on the basis of their 3D spatial structure (Figure 8(A)). After conformational overlap and alignment of the 5 binding conformations, we found that each loop contained several key residues whose side chains contributed to the formation of hydrogen bonds between the antigen and the mAb (Figure 8(E)). Several key residues were

highly conserved in the 5 binding conformations, including N23 and E35 in loop 1, D68 in loop 2, and D116 in loop 3 (Figure 8(E)). Although the other key residues varied among the different strains, they still participate in crucial hydrogen bonds for antibody binding. For example, when T122 in loop 3 was mutated to Y122, hydrogen bonds could still form between the hydroxyl group and the corresponding residue of the antibody (Figure 8(E)). This conserved

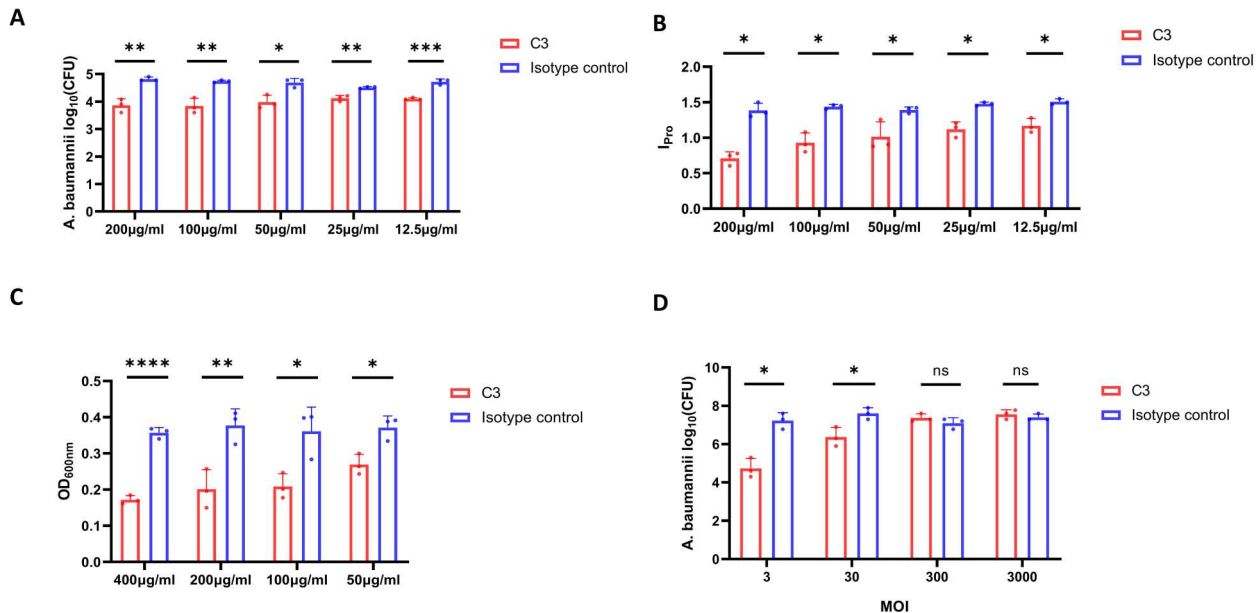


Figure 7. mAb C3 inhibited bacterial adhesion, intracellular proliferation, and biofilm formation and induced antibacterial sterilization. (A) Adherence of *A. baumannii* ATCC 17978 in the presence of the mAb C3 or the isotype control. A549 cells were infected with *A. baumannii* at an MOI of 1:100, and the mAb C3 or isotype control was added to the cell culture at the same time. The degree of bacterial adherence to A549 cells was quantified via the serial dilution method after the removal of external nonadherent bacteria. (B) Intracellular proliferation of *A. baumannii* ATCC 17978 in the presence of the mAb C3 or the isotype control. A549 cells were infected with *A. baumannii* at an MOI of 1:100, and the mAb C3 or isotype control was added to the cell culture at the same time. The intracellular proliferation rate (I_{pro}) was determined by calculating the number of viable intracellular bacteria present at 24 hours to those present at 4 hours postinfection. (C) Biofilm formation by ATCC 17978 in the presence of the mAb C3 or the isotype control. A total of 1.0×10^7 CFU/mL *A. baumannii* and mAb or isotype control were coinoculated for 26 hours at 37°C. The formed biofilm was then fixed with methanol for 20 minutes and stained with 0.1% crystal violet for 30 minutes. After washing with physiological saline, 95% ethanol was added to loosen the biofilm. Finally, the absorbance was measured at 600 nm via a microplate reader. (D) Opsonophagocytosis assay of C3 and the isotype control at different MOIs. *A. baumannii* strain LAC-4 was incubated with palmitoyl-2-cysteine-serine-lysine-4 (Pam₂CSK₄)-stimulated RAW264.7 cells at different MOIs (1:3, 1:30, 1:300, and 1:3000), and mAb C3 or an isotype control was added to the cell culture at the same time. After 5 hours of incubation with gentle shaking, the bacteria in the supernatant were verified via the serial dilution method. Each assay was performed in triplicate, and all the data are presented as the means \pm SEMs from three independent experiments. Comparisons of bacterial loads between the groups were carried out via unpaired Student's *t* test. ns: not significant; *, $P < 0.05$; **, $P < 0.01$; ***, $P < 0.001$; ****, $P < 0.0001$.

binding modality may explain the broad-spectrum binding activity of C3.

Discussion

In this study, we obtained several mAbs targeting the OMPs of *A. baumannii* using a high-throughput approach based on the Beacon platform. After Omp38-specific mAbs were identified, their binding activities with *A. baumannii* strains from diverse sources and their therapeutic efficacy in lethal and sublethal LAC-4 infection models were confirmed. Finally, we explored the potential mechanism by which C3 exhibits broad-spectrum binding.

Quality control was included during mAb production. Mouse immunization was performed in strict accordance with the instructions of the QuickAntibody Mouse3W (Biodragon, KX0210042), and the production of mAbs from immunized mice was confirmed via ELISA (Figure 1(C)). Before the Beacon on-chip assay, biotin detection was performed for quality control of the biotinylated OMPs, and the

results revealed that the OMPs were successfully labeled with biotin (Figure S5A). After the biotinylated OMPs were coupled to streptavidin-coated assay beads at 4°C overnight according to the Validation of Biotinylated Soluble Antigen Beads Protocol (MAN-000034), immunofluorescence was detected for quality control of the conjugated beads, and the results confirmed that the biotinylated OMPs were conjugated to the streptavidin-coated assay beads (Figure S5B). During the on-chip assay, the IgG beads were loaded into individual NanoPens on the chip to quantify the number of antibody-secreting plasma cells (Figure 2(B), right panel). Both OMP-reactive and IgG-reactive B cells were exported for further study to avoid false-positive results. Amplification of the VH and VL genes from the isolated cells was conducted in a strict ribonuclease (RNase)-free environment. For quality control of mAb expression and purification, ExpiCHO cells with a viable cell density greater than 50% and a cell viability rate greater than 60% were collected on the fifth day after mAb expression vector transfection. After purification, the

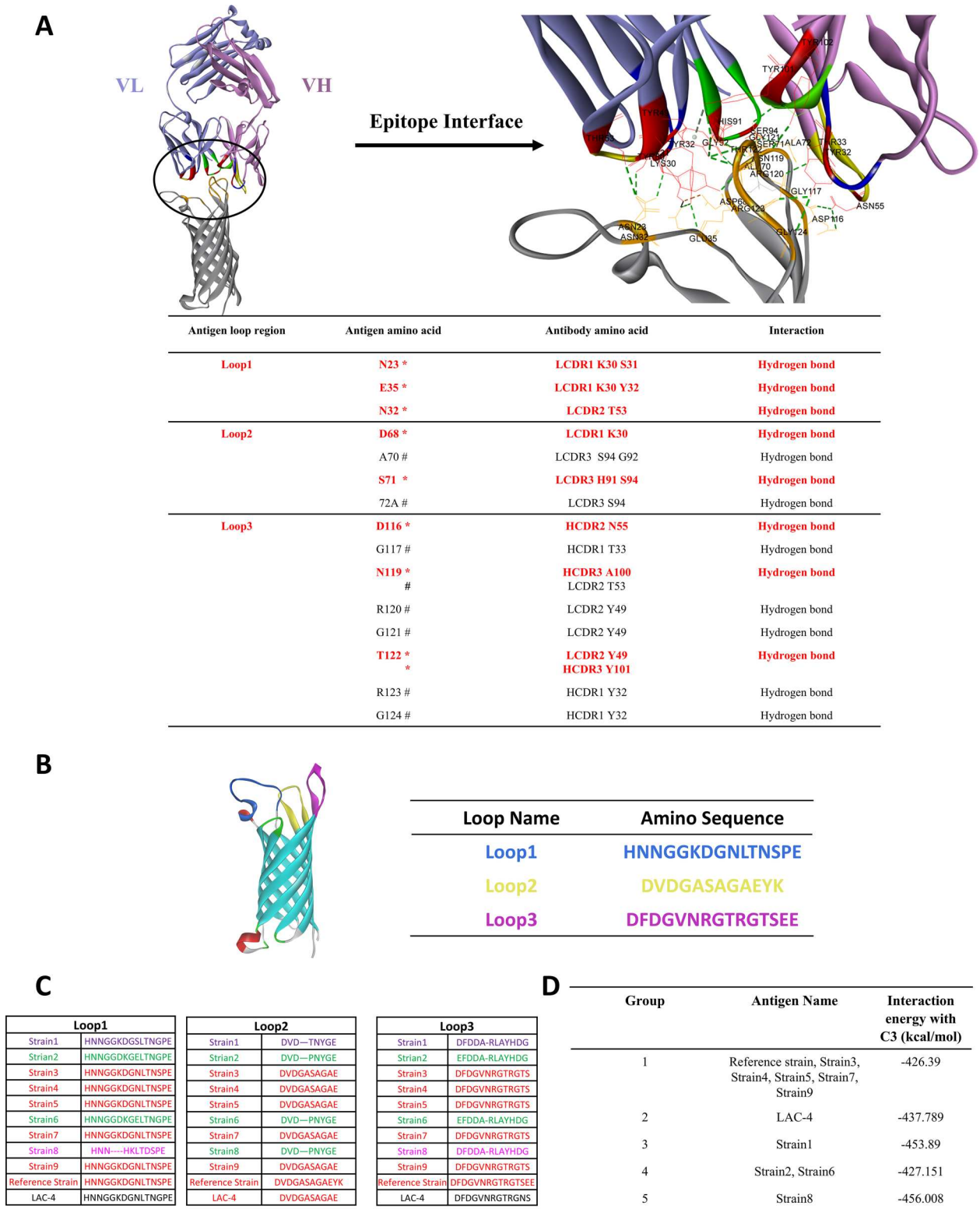


Figure 8. Predicted interaction between mAb C3 and *A. baumannii*. (A) Predicted binding between mAb C3 and the *A. baumannii* reference strain modeled by AlphaFold 3 and GeoBiologics. *, The side chain participates in hydrogen bonds; #, a group on the main protein chain participates in hydrogen bond formation. (B) The three loop regions of the Omp38 extracellular domain predicted by Discovery Studio 2.5. Loop 1, loop 2 and loop 3 are shown in blue, yellow, and pink, respectively. (C) Alignment of the loop region sequences from different strains on the basis of 3D structure by Discovery Studio 2.5 (Accelrys Software, Inc.). The key amino acids involved in antigen-antibody binding are labeled in red. (D) The binding energy between C3 and different strains of *A. baumannii* was calculated using CHARMM with the tools implemented in Discovery Studio 2.5 (Accelrys Software, Inc.). (E) Identification of the key residues in the 5 binding conformations by Discovery Studio 2.5 (Accelrys Software, Inc.). The key residues are shown in red. Group 1: reference strain, strain 3, strain 4, strain 5, strain 7, and strain 9. Group 2: LAC-4. Group 3: strain 1. Group 4: strain 2 and strain 6. Group 5: strain 8.

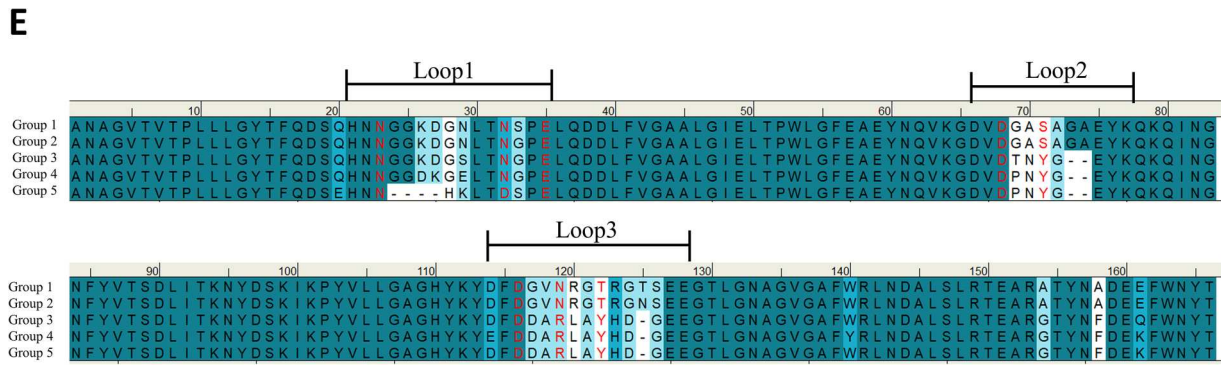


Figure 8. Continued.

yield of the mAbs was determined by a BCA protein concentration determination kit (Beyotime, P0012), and the purity of the mAbs was validated via SDS-PAGE (Figure S2). We also confirmed that the effect of the mAbs was stable. In this study, mAb C3 showed the best protective effect in both lethal and sublethal *A. baumannii* infection models, as well as high binding affinity for Omp38. In addition, we constructed a lethal *A. baumannii* infection model and confirmed the strong protective effect of C3. These results indicated that the effects of the mAbs were stable.

A. baumannii has emerged as a global concern because of its high virulence and pathogenicity; however, addressing antimicrobial resistance through the use of mAbs against this pathogen has become a common strategy. Recent studies have targeted Omp38 for developing antibodies against *A. baumannii* infection, although some limitations remain. Omid Yeganeh et al. utilized a peptide derived from *A. baumannii* Omp38 conjugated to keyhole limpet hemocyanin (KLH) for mouse immunization, resulting in IgG1 mAbs produced by hybridoma [39,58]. Although they validated the effects of the mAb *in vitro*, they did not explore its protective efficacy in animal models. In our study, both *in vitro* and *in vivo* experiments were conducted to confirm that Omp38-specific mAbs protected against lethal and sublethal *A. baumannii* infections. Research has demonstrated that mouse IgG1 binds only to the FcγRIIB and FcγRIII receptors [59], whereas mouse IgG2a mAbs can bind to the FcγRI, FcγRIIB, FcγRIII, and FcγRIV receptors [59]. Furthermore, mouse FcγRI and FcγRIV are expressed predominantly on monocytes and macrophages and exhibit high affinity interactions with IgG2a mAbs [59], which are crucial in *A. baumannii* infection. Thus, Omid Yeganeh et al. reported that IgG1 mAbs may result in unpredictable therapeutic effects *in vivo*. To validate our hypothesis, paired VH and VL sequences of selected mAbs, including F4, A2, C3, and G4, were codon optimized, synthesized by Shenggong Biotech, and cloned and inserted into separate mammalian expression vectors containing constant mouse IgG1 regions (Figure

S6A). We constructed a model of lethal LAC-4 infection under the same conditions as those used for the IgG2a-treated mice and treated the mice with 15 mg/kg IgG1 mAbs (Figure S6B). Notably, 3 out of the 4 candidate mAbs (F4, C3, and G4) delayed mouse death, whereas A2 did not have a protective effect against LAC-4 infection. Interestingly, a two-antibody cocktail (C3 + G4) at a final dosage of 15 mg/kg per mouse (7.5 mg/kg per antibody), resulted in a 16.7% survival rate (1 out of 6 mice) (Figure S6C). These results explained why IgG2a mAbs were chosen for our study. Hamideh Barati et al. generated immune serum through subcutaneous Omp38 immunization in mice, demonstrating the safety and efficacy of the antiserum in terms of bacterial killing, biofilm inhibition, and suppression of bacterial adhesion and intracellular proliferation [11]. However, their research developed mAbs, whereas our research identified mAbs targeting Omp38 in a high-throughput manner and validated their protective effects *in vitro* and *in vivo*.

The mechanisms of mAb-mediated protection against *A. baumannii* infection are not fully understood. Omp38-specific mAbs may activate Fcγ receptors on innate immune cells to trigger antibody effector functions other than ADCP, such as antibody-dependent cell-mediated cytotoxicity (ADCC), which refers infected cells coated with Omp38-specific mAbs being killed by effector cells of the immune system, such as NK cells [60]. In addition, Omp38-specific mAbs may also activate the complement cascade pathway to exert complement-dependent cytotoxicity (CDC) [61]. After the mAbs bound Omp38, the interaction between the crystallizable fragment (Fc) of the antibody and the first subcomponent of the C1 complement complex (C1q) activates the classical complement pathway, and the formation of the membrane attack complex (MAC) leads to the lysis of *A. baumannii*-infected cells [61].

While the Berkeley Lights Beacon platform offered significant advantages for rapid antibody isolation in this study, addressing its biological and technological limitations is essential. The platform's nanochip can

accommodate only 11,000 cells, which represents only a fraction of the total plasma cells isolated. The limited nanochip capacity restricts the throughput of single-cell analysis and reduces the probability of isolating antigen-specific B cells with very low frequency. Using nanochips accommodating more cells may solve this problem. Cell viability also plays an important role in the on-chip assay. The stability of RNA in plasma cells with low viability was reduced, which led to decreased VH and VL gene amplification efficiency. Therefore, shortening the time of the on-chip assays or developing more efficient culture media may solve these technical problems.

It has been reported that Omp38 is highly conserved in different *A. baumannii* strains [38], and our bioinformatic analysis results indicated the conservation of antibody binding epitopes among different strains, suggesting the broad effects of these mAbs. The predicted conformational epitopes of the mAbs in this study need further validation through more experiments, such as high-resolution cryo-EM analysis [50].

Conclusion

In conclusion, our study successfully identified 9 mAbs targeting OMPs in a high-throughput manner, 6 of which were Omp38-targeted mAbs that potently and broadly bound to 10 *A. baumannii* strains, and 4 of which could protect mice from infection. These findings provide new perspectives for the treatment of *A. baumannii* infection.

Future perspectives

With the development of genetic engineering technology, the humanization of mouse monoclonal antibodies has become an important approach to treat clinical diseases [62]. Transplanting the CDR region of nonhuman antibodies onto the framework region of human antibodies is a common method for preparing humanized antibodies [63,64]. Owing to the involvement of mouse hypervariable regions in the human antibody framework, 95% of these hybrid mAbs are human, with low immunogenicity and high affinity [62,65]. Future work will focus on their humanization, assessing their toxicity, generating a stably transfected master cell-bank clone, and establishing good manufacturing practice (GMP) production.

Acknowledgments

We thank Chao Han (Institute of Immunology, Third Military Medical University (Army Medical University), Chongqing 400038, People's Republic of China) and Mingyang Zhang (The Third Affiliated Hospital, Third Military Medical University (Army Medical University), Chongqing 400042, People's Republic of China) for their technical support. We thank Di Yang, Jian Zhou and Jingxue Wang

(Institute of Immunology, Third Military Medical University (Army Medical University), Chongqing 400038, People's Republic of China) for providing helpful and constructive comments that improved the manuscript substantially. We thank Shuai Xu (The Second Affiliated Hospital, Third Military Medical University (Army Medical University), Chongqing 400037, People's Republic of China) for their helpful comments about the data analysis.

Disclosure statement

No potential conflict of interest was reported by the author(s).

Funding

This work was supported by grants from the General Program of the National Natural Science Foundation of China (no. 32170887 and No. 31970885), the Special Program of the National Natural Science Foundation of China (no. 32141005), and the Major Research Plan of the National Natural Science Foundation of China (no. 92269110). Special fund for performance incentive guidance of research institutions in Chongqing (cstc2021jxj130036) and Chongqing International Institute for Immunology Project (2022YJC01). The funders had no role in the study design, data analyses, or decision to publish.

Author contributions

Yiwei Zhang: Writing – original draft, Investigation. Hao Cheng: Writing – original draft, Investigation. Peng Yu: Methodology, Supervision, Conceptualization. Shufeng Wang: Methodology, Supervision, Software. Hui Dong: Methodology, Validation. Song Lu: Methodology, Data curation. Ruiqi Yang: Methodology, Data curation. Baiqing Li: Methodology. Jie Luo: Methodology. Ruihan Mao: Validation. Zhaohui Zhang: Validation. Yong Qi: Methodology, Resources. Xiaohua Chen: Methodology, Resources. Jinya Ding: Resources. Zemin He: Resources. Jingbo Zhang: Resources. Tingting Zhao: Investigation, Methodology. Xiangmei Chen: Investigation, Methodology. Rong Lin: Investigation, Methodology. Haibo Li: Writing – review & editing, Project administration, Conceptualization. Yi Tian: Writing – review & editing, Project administration, Funding acquisition, Conceptualization. Yuzhang Wu: Writing – review & editing, Project administration, Conceptualization. All the authors reviewed and approved the final version of the manuscript.

References

- [1] Uppalapati SR, Sett A, Pathania R. The outer membrane proteins OmpA, CarO, and OprD of *Acinetobacter baumannii* confer a two-pronged defense in facilitating its success as a potent human pathogen. *Front Microbiol.* 2020;11:589234. doi:10.3389/fmicb.2020.589234
- [2] Zhou H, Yao Y, Zhu B, et al. Risk factors for acquisition and mortality of multidrug-resistant

- Acinetobacter baumannii bacteremia: A retrospective study from a Chinese hospital. *Medicine*. 2019;98(13):e14937. doi:10.1097/MD.00000000000014937
- [3] Garnacho-Montero J, Dimopoulos G, Poulakou G, et al. Task force on management and prevention of Acinetobacter baumannii infections in the ICU. *Intensive Care Med*. 2015;41(12):2057–2075. doi:10.1007/s00134-015-4079-4
 - [4] Dijkshoorn L, Nemec A, Seifert H. An increasing threat in hospitals: multidrug-resistant Acinetobacter baumannii. *Nat Rev Microbiol*. 2007;5(12):939–951. doi:10.1038/nrmicro1789
 - [5] Singh R, Capalash N, Sharma P. Vaccine development to control the rising scourge of antibiotic-resistant Acinetobacter baumannii: a systematic review. *3 Biotech*. 2022;12(3):85. doi:10.1007/s13205-022-03148-9
 - [6] Broad J, Le Doare K, Heath PT, et al. The current state of immunization against Gram-negative bacteria in children: a review of the literature. *Curr Opin Infect Dis*. 2020;33(6):517–529. doi:10.1097/QCO.0000000000000687
 - [7] Ma C, McClean S. Mapping global prevalence of Acinetobacter baumannii and recent vaccine development to tackle it. *Vaccines*. 2021;9(6):570. doi:10.3390/vaccines9060570
 - [8] Nielsen TB, Pantapalangkoor P, Luna BM, et al. Monoclonal antibody protects against Acinetobacter baumannii infection by enhancing bacterial clearance and evading sepsis. *J Infect Dis*. 2017;216(4):489–501. doi:10.1093/infdis/jix315
 - [9] Goel VK, Kapil A. Monoclonal antibodies against the iron regulated outer membrane proteins of Acinetobacter baumannii are bactericidal. *BMC Microbiol*. 2001;1(1):16. doi:10.1186/1471-2180-1-16
 - [10] Naghipour Erami A, Rasooli I, Jahangiri A, et al. Anti-Omp34 antibodies protect against Acinetobacter baumannii in a murine sepsis model. *Microb Pathog*. 2021;161:105291. doi:10.1016/j.micpath.2021.105291
 - [11] Barati H, Fekrirad Z, Jalali Nadoushan M, et al. Anti-OmpA antibodies as potential inhibitors of Acinetobacter baumannii biofilm formation, adherence to, and proliferation in A549 human alveolar epithelial cells. *Microb Pathog*. 2024;186:106473. doi:10.1016/j.micpath.2023.106473
 - [12] McConnell MJ. Where are we with monoclonal antibodies for multidrug-resistant infections? *Drug Discov Today*. 2019;24(5):1132–1138. doi:10.1016/j.drudis.2019.03.002
 - [13] Pedrioli A, Oxenius A. Single B cell technologies for monoclonal antibody discovery. *Trends Immunol*. 2021;42(12):1143–1158. doi:10.1016/j.it.2021.10.008
 - [14] Kessler N, Bertrand S, Aymard M. Stability of a murine hybridoma is dependent on the clonal line and culture media. *In Vitro Cell Dev Biol*. 1993;29A(3):203–207. doi:10.1007/BF02634184
 - [15] Mahdavi SZB, Oroojalian F, Eyvazi S, et al. An overview on display systems (phage, bacterial, and yeast display) for production of anticancer antibodies; advantages and disadvantages. *Int J Biol Macromol*. 2022;208:421–442. doi:10.1016/j.ijbiomac.2022.03.113
 - [16] Yu P, Ran J, Yang R, et al. Rapid isolation of pan-neutralizing antibodies against Omicron variants from convalescent individuals infected with SARS-CoV-2. *Front Immunol*. 2024;15:1374913. doi:10.3389/fimmu.2024.1374913
 - [17] Hoogenboom HR. Overview of antibody phage-display technology and its applications. *Methods Mol Biol*. 2002;178:1–37.
 - [18] Fitzgerald V, Leonard P. Single cell screening approaches for antibody discovery. *Methods*. 2017;116:34–42. doi:10.1016/j.jymeth.2016.11.006
 - [19] Seah YFS, Hu H, Merten CA. Microfluidic single-cell technology in immunology and antibody screening. *Mol Aspects Med*. 2018;59:47–61. doi:10.1016/j.mam.2017.09.004
 - [20] Voigt A, Semenova T, Yamamoto J, et al. Therapeutic antibody discovery in infectious diseases using single-cell analysis. *Adv Exp Med Biol*. 2018;1068:89–102. doi:10.1007/978-981-13-0502-3_8
 - [21] Valley JK, Neale S, Hsu HY, et al. Parallel single-cell light-induced electroporation and dielectrophoretic manipulation. *Lab Chip*. 2009;9(12):1714–1720. doi:10.1039/b821678a
 - [22] Chiou PY, Ohta AT, Wu MC. Massively parallel manipulation of single cells and microparticles using optical images. *Nature*. 2005;436(7049):370–372. doi:10.1038/nature03831
 - [23] Hsu HY, Ohta AT, Chiou PY, et al. Phototransistor-based optoelectronic tweezers for dynamic cell manipulation in cell culture media. *Lab Chip*. 2010;10(2):165–172. doi:10.1039/B906593H
 - [24] Valley JK, Jamshidi A, Ohta AT, et al. Operational regimes and physics present in optoelectronic tweezers. *J Microelectromech Syst*. 2008;17(2):342–350. doi:10.1109/JMEMS.2008.916335
 - [25] Bhattacharyya T, Sharma A, Akhter J, et al. The small molecule IITR08027 restores the antibacterial activity of fluoroquinolones against multidrug-resistant Acinetobacter baumannii by efflux inhibition. *Int J Antimicrob Agents*. 2017;50(2):219–226. doi:10.1016/j.ijantimicag.2017.03.005
 - [26] Iyer R, Moussa SH, Durand-Reville TF, et al. Acinetobacter baumannii OmpA is a selective antibiotic permeant porin. *ACS Infect Dis*. 2018;4(3):373–381. doi:10.1021/acscinfecdis.7b00168
 - [27] Zhang MN, Zhao XO, Cui Q, et al. Famotidine enhances rifampicin activity against Acinetobacter baumannii by affecting OmpA. *J Bacteriol*. 2023;205:e0018723.
 - [28] Li Y, Peng C, Zhao D, et al. Outer membrane protein A inhibits the degradation of caspase-1 to regulate NLRP3 inflammasome activation and exacerbate the Acinetobacter baumannii pulmonary inflammation. *Microb Pathog*. 2021;153:104788. doi:10.1016/j.micpath.2021.104788
 - [29] Nie D, Hu Y, Chen Z, et al. Outer membrane protein A (OmpA) as a potential therapeutic target for Acinetobacter baumannii infection. *J Biomed Sci*. 2020;27(1):26. doi:10.1186/s12929-020-0617-7
 - [30] Sanchez-Encinales V, Alvarez-Marin R, Pachon-Ibanez ME, et al. Overproduction of outer membrane protein A by Acinetobacter baumannii as a risk factor for nosocomial pneumonia, bacteremia, and mortality rate increase. *J Infect Dis*. 2017;215:966–974.
 - [31] Wessel D, Flugge UI. A method for the quantitative recovery of protein in dilute solution in the presence of detergents and lipids. *Anal Biochem*. 1984;138(1):141–143. doi:10.1016/0003-2697(84)90782-6
 - [32] Nguyen DC, Garimalla S, Xiao H, et al. Factors of the bone marrow microniche that support human plasma

- cell survival and immunoglobulin secretion. *Nat Commun.* 2018;9(1):3698. doi:10.1038/s41467-018-05853-7
- [33] Liu C, Luo J, Xue RY, et al. The mucosal adjuvant effect of plant polysaccharides for induction of protective immunity against *Helicobacter pylori* infection. *Vaccine.* 2019;37(8):1053–1061. doi:10.1016/j.vaccine.2018.12.066
- [34] Hatefi Oskuei R, Darvish Alipour Astaneh S, Rasooli I. A conserved region of *Acinetobacter* trimeric autotransporter adhesion, Ata, provokes suppression of *Acinetobacter baumannii* virulence. *Arch Microbiol.* 2021;203(6):3483–3493. doi:10.1007/s00203-021-02343-1
- [35] Cano DA, Martinez-Moya M, Pucciarelli MG, et al. *Salmonella enterica* serovar Typhimurium response involved in attenuation of pathogen intracellular proliferation. *Infect Immun.* 2001;69(10):6463–6474. doi:10.1128/IAI.69.10.6463-6474.2001
- [36] Rajabzadeh M, Fekrirad Z, Jalali Nadoushan M, et al. Characterizing the interplay between *Acinetobacter baumannii*, A549 cells, and anti-Omp34 antibodies: implications for adherence, internalization, and cytotoxicity. *Folia Microbiol (Praha).* 2024.
- [37] Momeni M, Fekrirad Z, Jalali Nadoushan M, et al. Targeting BamA, the essential component of the *Acinetobacter baumannii* beta-barrel assembly machinery, hinders its ability to adhere to and invade human alveolar basal epithelial cell line. *Heliyon.* 2024;10:e34371. doi:10.1016/j.heliyon.2024.e34371
- [38] Luo G, Lin L, Ibrahim AS, et al. Active and passive immunization protects against lethal, extreme drug resistant-*Acinetobacter baumannii* infection. *PLoS One.* 2012;7(1):e29446. doi:10.1371/journal.pone.0029446
- [39] Yeganeh O, Shabani M, Pakzad P, et al. Evaluation the reactivity of a peptide-based monoclonal antibody derived from OmpA with drug resistant pulsotypes of *Acinetobacter baumannii* as a potential therapeutic approach. *Ann Clin Microbiol Antimicrob.* 2022;21:30. doi:10.1186/s12941-022-00523-5
- [40] de Campos GY, Oliveira RA, Oliveira-Brito PKM, et al. Pro-inflammatory response ensured by LPS and Pam3CSK4 in RAW 264.7 cells did not improve a fungistatic effect on *Cryptococcus gattii* infection. *PeerJ.* 2020;8:e10295. doi:10.7717/peerj.10295
- [41] Li S, Chen DQ, Ji L, et al. Development of different methods for preparing *Acinetobacter baumannii* outer membrane vesicles vaccine: impact of preparation method on protective efficacy. *Front Immunol.* 2020;11:1069. doi:10.3389/fimmu.2020.01069
- [42] Gu H, Liu D, Zeng X, et al. Aging exacerbates mortality of *Acinetobacter baumannii* pneumonia and reduces the efficacies of antibiotics and vaccine. *Aging.* 2018;10(7):1597–1608. doi:10.18632/aging.101495
- [43] Gurusamy M, Nasser S, Rampa DR, et al. Inhibition of microsomal prostaglandin E synthase-1 ameliorates acute lung injury in mice. *J Transl Med.* 2021;19(1):340. doi:10.1186/s12967-021-03016-9
- [44] Nasser S, Gurusamy M, Jung B, et al. Kinin B1 receptor antagonist BII13823 reduces acute lung injury. *Crit Care Med.* 2015;43(11):e499–e507. doi:10.1097/CCM.0000000000001268
- [45] Jia K, Zhang Y, Jiang M, et al. Dual-antigen fusion protein vaccination induces protective immunity against *Candida albicans* infection in mice. *Hum Vaccin Immunother.* 2024;20(1):2406065. doi:10.1080/21645515.2024.2406065
- [46] Diancourt L, Passet V, Nemec A, et al. The population structure of expanding multidrug-resistant clones from an ancestral susceptible genetic pool. *PLoS One.* 2010;5(4):e10034. doi:10.1371/journal.pone.0010034
- [47] Ou HY, Kuang SN, He X, et al. Complete genome sequence of hypervirulent and outbreak-associated *Acinetobacter baumannii* strain LAC-4: epidemiology, resistance genetic determinants and potential virulence factors. *Sci Rep.* 2015;5(1):8643. doi:10.1038/srep08643
- [48] El-Shazly S, Dashti A, Vali L, et al. Molecular epidemiology and characterization of multiple drug-resistant (MDR) clinical isolates of *Acinetobacter baumannii*. *Int J Infect Dis.* 2015;41:42–49. doi:10.1016/j.ijid.2015.10.016
- [49] McConnell MJ, Dominguez-Herrera J, Smani Y, et al. Vaccination with outer membrane complexes elicits rapid protective immunity to multidrug-resistant *Acinetobacter baumannii*. *Infect Immun.* 2011;79(1):518–526. doi:10.1128/IAI.00741-10
- [50] Zheng Q, Zhu R, Yin Z, et al. Structural basis for the synergistic neutralization of coxsackievirus B1 by a triple-antibody cocktail. *Cell Host Microbe.* 2022;30(9):1279–1294.e6. doi:10.1016/j.chom.2022.08.001
- [51] Garcia-Patino MG, Garcia-Contreras R, Licon-Limon P. The immune response against *Acinetobacter baumannii*, an emerging pathogen in nosocomial infections. *Front Immunol.* 2017;8:441. doi:10.3389/fimmu.2017.00441
- [52] Zarrilli R. *Acinetobacter baumannii* virulence determinants involved in biofilm growth and adherence to host epithelial cells. *Virulence.* 2016;7(4):367–368. doi:10.1080/21505594.2016.1150405
- [53] Gaddy JA, Tomaras AP, Actis LA. The *Acinetobacter baumannii* 19606 OmpA protein plays a role in biofilm formation on abiotic surfaces and in the interaction of this pathogen with eukaryotic cells. *Infect Immun.* 2009;77(8):3150–3160. doi:10.1128/IAI.00096-09
- [54] Halstead SB, Mahalingam S, Marovich MA, et al. Intrinsic antibody-dependent enhancement of microbial infection in macrophages: disease regulation by immune complexes. *Lancet Infect Dis.* 2010;10(10):712–722. doi:10.1016/S1473-3099(10)70166-3
- [55] Qiu H, KuoLee R, Harris G, et al. Role of macrophages in early host resistance to respiratory *Acinetobacter baumannii* infection. *PLoS One.* 2012;7(6):e40019. doi:10.1371/journal.pone.0040019
- [56] Madsen AV, Mejias-Gomez O, Pedersen LE, et al. Structural trends in antibody-antigen binding interfaces: a computational analysis of 1833 experimentally determined 3D structures. *Comput Struct Biotechnol J.* 2024;23:199–211. doi:10.1016/j.csbj.2023.11.056
- [57] Yoshida K, Kuroda D, Kiyoshi M, et al. Exploring designability of electrostatic complementarity at an antigen-antibody interface directed by mutagenesis, biophysical analysis, and molecular dynamics simulations. *Sci Rep.* 2019;9(1):4482. doi:10.1038/s41598-019-40461-5
- [58] Yeganeh O, Shabani M, Pakzad P, et al. Production and characterization of novel monoclonal antibodies against outer membrane protein A (OmpA) of

- Acinetobacter baumannii. *J Immunol Methods*. 2021;499:113169. doi:10.1016/j.jim.2021.113169
- [59] Lux A, Nimmerjahn F. Of mice and men: the need for humanized mouse models to study human IgG activity in vivo. *J Clin Immunol*. 2013;33(S1):4–8. doi:10.1007/s10875-012-9782-0
- [60] Ochoa MC, Minute L, Rodriguez I, et al. Antibody-dependent cell cytotoxicity: immunotherapy strategies enhancing effector NK cells. *Immunol Cell Biol*. 2017;95(4):347–355. doi:10.1038/icb.2017.6
- [61] Wang B, Yang C, Jin X, et al. Regulation of antibody-mediated complement-dependent cytotoxicity by modulating the intrinsic affinity and binding valency of IgG for target antigen. *MAbs*. 2020;12(1):1690959. doi:10.1080/19420862.2019.1690959
- [62] Alejandra WP, Miriam Irene JP, Fabio Antonio GS, et al. Production of monoclonal antibodies for therapeutic purposes: a review. *Int Immunopharmacol*. 2023;120:110376. doi:10.1016/j.intimp.2023.110376
- [63] Jin KT, Chen B, Liu YY, et al. Monoclonal antibodies and chimeric antigen receptor (CAR) T cells in the treatment of colorectal cancer. *Cancer Cell Int*. 2021;21(1):83. doi:10.1186/s12935-021-01763-9
- [64] Waldmann H. Human monoclonal antibodies: the benefits of humanization. *Methods Mol Biol*. 2019;1904:1–10. doi:10.1007/978-1-4939-8958-4_1
- [65] Bayer V. An overview of monoclonal antibodies. *Semin Oncol Nurs*. 2019;35(5):150927. doi:10.1016/j.soncn.2019.08.006